nature neuroscience

ARTICLES

https://doi.org/10.1038/s41593-020-0674-y

Check for updates

Social touch promotes interfemale communication via activation of parvocellular oxytocin neurons

Yan Tang[1,9,10], Diego Benusiglio[1,10], Arthur Lefevre[1,2,10], Louis Hilfiger[2,10], Ferdinand Althammer[1,3], Anna Bludau[4], Daisuke Hagiwara[1], Angel Baudon[2], Pascal Darbon[2], Jonas Schimmer[1], Matthew K. Kirchner[3], Ranjan K. Roy[3], Shiyi Wang[1], Marina Eliava[1], Shlomo Wagner[5], Martina Oberhuber[6], Karl K. Conzelmann[6], Martin Schwarz[7], Javier E. Stern[3], Gareth Leng[8], Inga D. Neumann[4,11], Alexandre Charlet[2,11] ✉ and Valery Grinevich[1,3,11] ✉

Oxytocin (OT) is a great facilitator of social life but, although its effects on socially relevant brain regions have been extensively studied, OT neuron activity during actual social interactions remains unexplored. Most OT neurons are magnocellular neurons, which simultaneously project to the pituitary and forebrain regions involved in social behaviors. In the present study, we show that a much smaller population of OT neurons, parvocellular neurons that do not project to the pituitary but synapse onto magnocellular neurons, is preferentially activated by somatosensory stimuli. This activation is transmitted to the larger population of magnocellular neurons, which consequently show coordinated increases in their activity during social interactions between virgin female rats. Selectively activating these parvocellular neurons promotes social motivation, whereas inhibiting them reduces social interactions. Thus, parvocellular OT neurons receive particular inputs to control social behavior by coordinating the responses of the much larger population of magnocellular OT neurons.

The hypothalamic neuropeptide OT promotes various types of social behavior[1–3]. OT is mainly synthesized in neurons of the paraventricular nuclei (PVN) and supraoptic nuclei (SON) of the hypothalamus. The vast majority of these neurons project to the posterior pituitary, where OT is secreted into the blood for essential physiological effects, such as suckling-induced milk letdown and regulation of uterine contractions during birth[4]. In parallel, these neurons project axonal collaterals to forebrain regions[5] that express OT receptors (OTRs), including the central nucleus of the amygdala, nucleus accumbens, lateral septum, hippocampus and medial prefrontal cortex[6,7]. Studies employing microdialysis to measure OT concentrations within socially relevant brain regions revealed that OT is released in the bed nucleus of the stria terminalis, lateral septum and central nucleus of the amygdala during social investigation of a conspecific[2,8,9]. However, to date, no direct measurement of OT neuron activity during actual social interaction of freely moving conspecifics has been performed, although it was recently reported that social approach triggers calcium release in PVN OT neurons in immobilized, head-fixed male mice[10].

Several studies suggest that female–female interactions are predominantly mediated via somatosensory inputs[11,12], whereas other interactions such as male–male, male–female or parental contact may rely on other sensory modalities. However, whether these sensory stimulations can activate OT neurons is unknown because, to date, there has been no direct recording of activity from identified OT neurons during actual social behavior. In an attempt to address these points, in the present study, we performed ex vivo and in vivo manipulation of OT neuron activity primarily in the PVN—the main source of OT in the brain[5]—to decipher their involvement in the modulation of social interaction in freely moving female rats.

Results

PVN OT neurons are activated on social interaction. To identify OT neurons electrophysiologically, we injected a recombinant adeno-associated virus (rAAV-OTp-ChR2-mCherry) bilaterally into the PVN to induce expression of the light-sensitive ion channel Channelrhodopsin-2 (ChR2) under the control of the OT promoter[5,13]. This resulted in 90.4% of ChR2-expressing neurons being OT positive, showing the high specificity of the infection in the PVN (Extended Data Fig. 1a). We then recorded individual neurons in the PVN using implanted tetrodes combined with an optic fiber to identify the OT neurons by their electrophysiological response to blue-laser pulses, similar to methods described previously[14].

In total, we recorded 90 neurons in 10 adult female rats at the diestrus phase of the ovarian cycle, while monitoring the behavior of the rats and their ultrasonic vocalizations during both open field (OF) exploration and free social interactions (FSIs) (Fig. 1a,b). Of these neurons, 15 (in 5 animals) were stringently identified as single OT neurons (Extended Data Fig. 1e). In the OF arena, the patterns of spiking activity of these neurons (Fig. 1d and Extended

[1]Department of Neuropeptide Research in Psychiatry, Central Institute of Mental Health, Medical Faculty Mannheim, University of Heidelberg, Mannheim, Germany. [2]Centre National de la Recherche Scientifique, Institute of Cellular and Integrative Neurosciences, University of Strasbourg, Strasbourg, France. [3]Center for Neuroinflammation and Cardiometabolic Diseases, Georgia State University, Atlanta, GA, USA. [4]Department of Neurobiology and Animal Physiology, University of Regensburg, Regensburg, Germany. [5]Sagol Department of Neurobiology, University of Haifa, Mount Carmel, Haifa, Israel. [6]Max von Pettenkofer-Institute Virology, Faculty of Medicine and Gene Center, Ludwig Maximilian University, Munich, Germany. [7]Institute for Experimental Epileptology and Cognition Research, University of Bonn Medical Center, Bonn, Germany. [8]Centre for Discovery Brain Sciences, University of Edinburgh, Edinburgh, UK. [9]Present address: Centre de Neurosciences Psychiatriques, Centre Hospitalier Universitaire Vaudois (CHUV) , Prilly (Lausanne), Switzerland. [10]These authors contributed equally: Yan Tang, Diego Benusiglio, Arthur Lefevre, Louis Hilfiger. [11]These authors jointly supervised this work: Inga D. Neumann, Alexandre Charlet, Valery Grinevich. ✉e-mail: acharlet@unistra.fr; valery.grinevich@zi-mannheim.de

Data Fig. 2d) were indistinguishable from those of OT neurons observed under basal conditions in anesthetized rats, because these neurons displayed typical OT neuron characteristics[15]. Specifically, they all display a low rate of tonic firing (~1 Hz) with a low index of dispersion of spikes (<1), and a distribution of interspike intervals consistent with random spike generation subject to a prolonged relative refractory period. In contrast, during episodes of FSI with an unfamiliar conspecific, the same neurons fired at a higher rate (mean increase 1.5 ± 0.4 spikes s^{-1}, $P = 0.001$, $n = 15$; Fig. 1c,d) and more irregularly; the second-by-second firing rates showed a high index of dispersion, reflecting the prominent occurrence of clusters of spikes (Fig. 1d and Extended Data Fig. 1n).

As revealed by cross-correlation analysis, OT neurons also displayed increased synchronicity during FSI (mean pairwise correlation: OF, 0.10 ± 0.04; FSI, 0.40 ± 0.08, $P = 0.001$; Extended Data Fig. 1k–l). In anesthetized rats, adjacent OT neurons showed no such cross-correlated activity. We also recorded local field potentials in the PVN and found a substantial increase of oscillatory power in the theta (5–10 Hz) frequency band during FSI (Extended Data Fig. 1f–h). The spike activity of OT neurons tended to be phase-locked with theta oscillations during FSI, but not in the OF arena (Extended Data Fig. 1i,j). In contrast to OT neurons, non-OT PVN neurons did not show an increase in spiking activity when comparing exploratory behavior and social interaction (Extended Data Fig. 2e–g).

Thus, during FSI with actual physical contact, OT neurons in the PVN were more active and exhibited frequent clusters of spikes, and this activity was correlated among the OT neurons.

Social physical contact increases PVN OT neuron activity. To examine which component of social interaction activates these neurons, we first recorded their neuronal activity during a chambered social interaction (CSI)[16]. In this setup, experimental and stimulus rats were separated by a transparent wall with small holes (7.5 mm), allowing rats to see, sniff and hear, but not touch, each other (Fig. 1e).

OT neurons showed little change in spiking activity between CSI and baseline recordings in an OF (CSI: 1.4 ± 0.4 spikes s^{-1}; OF: 1.0 ± 0.2 spikes s^{-1}, $P = 0.14$; Fig. 1f). When the wall was removed to allow FSI, the same OT neurons displayed a significant increase in activity (FSI: 3.0 ± 0.4 spikes s^{-1}, $P < 0.001$; Fig. 1f), accompanied by an increase in index of dispersion (FSI 3.2 ± 0.4, CSI 1.3 ± 0.3, $P = 0.006$ versus FSI; OF 0.9 ± 0.2, $P = 0.004$ versus FSI). To estimate the amount of OT axonal release due to the increase in firing rate, together with the altered firing pattern, we employed an activity (spike)-dependent model of OT secretion[17] (Extended Data Fig. 2h–j) that quantitatively captures the features of stimulus secretion coupling at the nerve terminals.

To dissect which sensory modalities activate OT neurons during FSI, we categorized rat social behaviors into 'sniffing', 'head-to-head' and 'crawled on top' or 'being crawled' events and constructed peristimulus time histograms (PSTHs) of spiking activity before, during and after the onset of each sequence (Fig. 1g,h). 'Crawled on top' and 'being crawled' induced the greatest increases in firing rates ($P = 0.036$ and 0.024, respectively; Supplementary Video 1), whereas 'sniffing', 'chasing' and 'head-to-head' events induced lesser, non-significant changes (Fig. 1h and Extended Data Fig. 2a–c). In addition, ultrasonic vocalizations during FSI revealed the appearance of bands between 40 and 90 kHz known to be related to social communication in rats[18] (Extended Data Fig. 3a,b), but we found no time-locked (in ranges up to ±5 s) correlation between OT neuron activity and ultrasonic vocalizations (Extended Data Fig. 3c–e). Although we could not discriminate individual ultrasonic vocalizations between the two conspecifics, we hypothesized that OT neurons were activated mainly by physical contacts and investigated this further by modeling gentle, non-nociceptive mechanical stimuli.

Gentle non-nociceptive mechanical stimuli trigger OT neuron activation. To test whether somatosensory stimulation itself is sufficient to increase OT cell activity, we performed controlled tactile stimulations using compressed air delivery (airpuffs) in isoflurane-anesthetized rats as described previously[19] (Fig. 2a). Stimulation of the skin on the dorsal body region by airpuffs (at three sites) reproducibly activated 19 of 23 (83%) recorded PVN OT neurons (mean increase 1.3 ± 0.5 spikes s^{-1}, mean $P = 0.021$; Fig. 2a,b and Extended Data Fig. 4a,b).

Airpuffs applied to the abdominal skin produced few or no changes in their activity (mean change 0.5 ± 0.3 spikes s^{-1}, $P = 0.33$), and there were no detected effects after stimulation of the anogenital area or the whiskers pad (Extended Data Fig. 4c). For potential involvement of the olfactory system in PVN OT neuron activation during social interaction, we exposed female rats to either a neutral odor (clean bedding) or a socially relevant odor (urinated-on female bedding). We found that the exposure to odorants did not elicit significant changes in either firing rate or spike distribution ($P = 0.34$ or 0.48, respectively; Extended Data Fig. 4d–f) in any of the recorded OT neurons. There was also no difference on presentation of neutral odor. Hence, we concluded that somatosensory inputs are the dominant signals that activate PVN OT neurons during social interactions.

ParvOT neurons respond to gentle non-nociceptive mechanical stimuli. Although the overwhelming majority of OT neurons in the PVN (97%) are magnocellular OT (magnOT) neurons, there is also a population of parvocellular OT (parvOT) neurons (~3%) that do not project to the pituitary[20], but that are crucial for the transmission of nociceptive signals to the magnOT cells[13].

Fig. 1 | In vivo recording of individual OT neurons in the PVN. a, Setup for recordings of behavior, ultrasonic vocalizations and neural activity. **b**, Video-tracking and electrophysiological recording from a rat alone in the OF arena (top) and during FSI (bottom): animal movement path (blue line), location of prominent OT cell activity (colored dots), heatmap of time spent by the rat in different locations. **c**, Example firing rate of four identified OT neurons recorded simultaneously during FSI. Red bars indicate periods of social interaction. **d**, Average firing rate of 15 OT neurons from 5 rats: OF baseline 1.1 ± 0.4 Hz, not socially interacting (not-SI) 1.6 ± 0.3 Hz and SI 2.6 ± 0.2 Hz (OF not-SI, $P = 0.07$; OF SI, $P = 0.001$; not-SI SI, $P = 0.03$; one-way ANOVA). Average index of dispersion on 1-s time bins of 15 OT neurons: OF 0.9 ± 0.2, not-SI 1.4 ± 0.3, SI 3.4 ± 0.4 (OF not-SI, $P = 0.16$; OF SI, $P = 0.0004$; not-SI SI, $P = 0.001$; one-way ANOVA). Average pairwise Pearson's correlation of spiking activity (1-s time bins) of 17 OT neuron pairs recorded in OF and SI ($P = 0.005$, unpaired, two-sided Student's *t*-test). **e**, Frames of recorded videos (top) of experimental rats that were placed either alone (OF), or with a mesh between rats (CSI) or for FSI with a stimulus rat; representative spike raster plots of an OT cell in each condition (bottom). **f**, Average firing rate of 15 OT neurons while rats underwent OF, CSI and FSI tests (OF CSI $P = 0.14$; OF FSI, $P = 0.004$; CSI FSI, $P = 0.006$; $n = 15$ cells; one-way ANOVA). Average index of dispersion on 1-s time bins (OF CSI, $P = 0.21$; OF FSI, $P = 0.001$; CSI FSI, $P = 0.003$; $n = 15$ cells; one-way ANOVA). Average pairwise Pearson's correlation of spiking activity (1-s time bins) of 17 OT neuron pairs (OF CSI, $P = 0.39$; OF FSI, $P = 0.002$; CSI FSI, $P = 0.003$; one-way ANOVA). **g**, Normalized firing rates of OT neurons during each behavior; 'crawling on top' and 'being crawled' elicited the strongest responses (*$P = 0.036$, **$P = 0.024$; $n = 8$ cells, one-way ANOVA, followed by Tukey's post hoc test). **h**, Representative spike raster plots, averaged response and PSTHs of OT cell activity during 'crawling on top' (increased response, $P = 0.036$, $n = 6$ cells, Wilcoxon's test) and 'being crawled' (increased response, $P = 0.024$, $n = 6$ cells; Wilcoxon's test) behaviors. Data represented as mean ± s.e.m.

To study whether parvOT neurons are also activated by non-nociceptive stimuli, we applied airpuffs to conscious rats trained and adapted for short-term immobilization. For this purpose, we first used rats that had been injected systemically with the retrograde tracer Fluorogold to label all neurons in the brain that project outside the blood–brain barrier, including in particular magnOT,

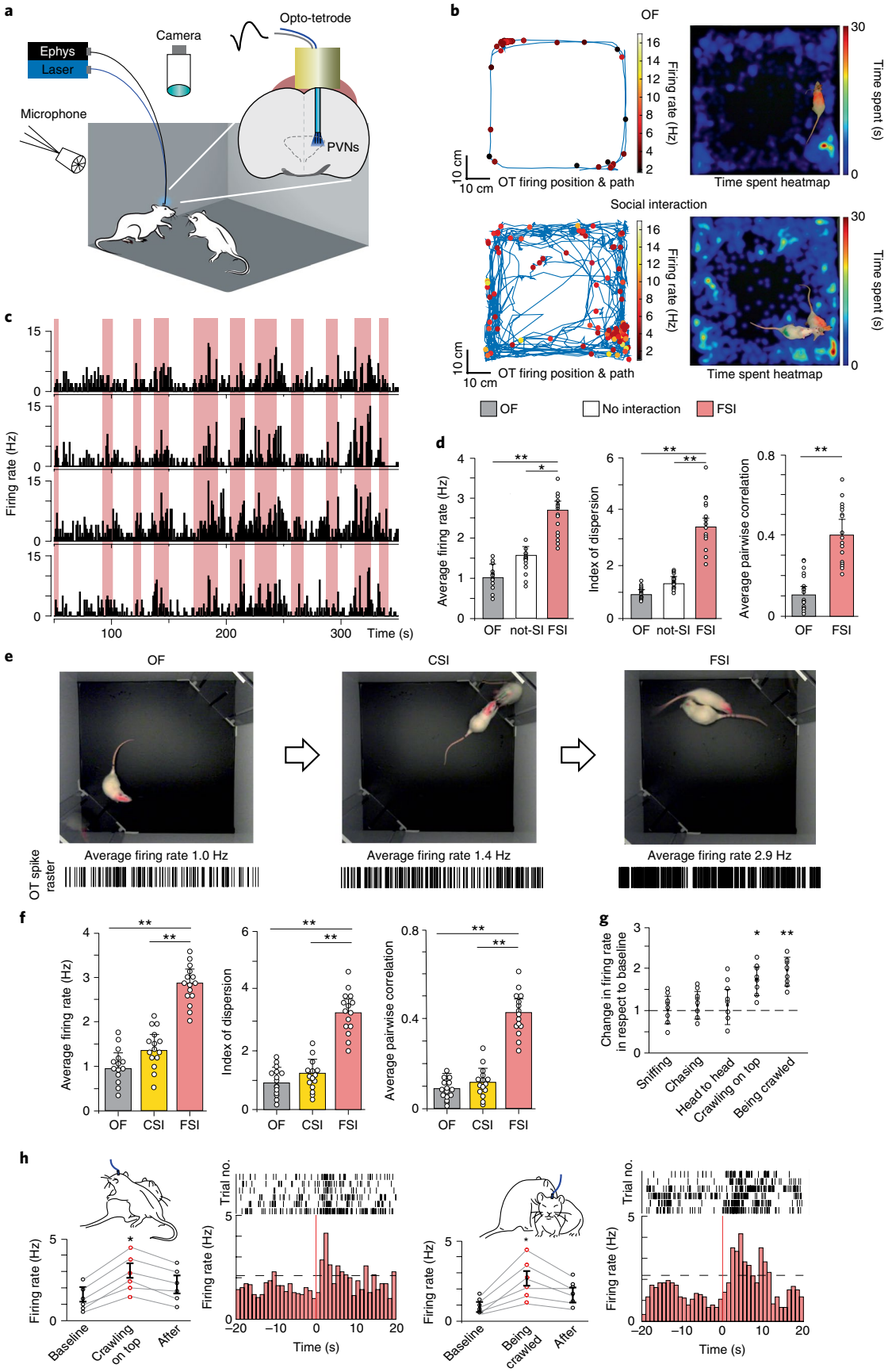

but not parvOT, neurons. To identify neurons strongly activated by airpuffs, we used the expression of *c-fos* as an indicator of activated OT neurons. Previous studies have found that *c-fos* expression is activated in a non-identified OT neuron cell type after social interaction in voles[21], mice[22] and rats[23]. Immunocytochemistry revealed the presence of *c-fos* in 30% of parvOT neurons in the PVN of stimulated rats (average 12.4 ± 3 neurons per PVN per hemisphere, $n = 4$; Fig. 2c and Supplementary Table 1a), but not in magnOT neurons or in any OT neurons in nonstimulated control rats, indicating that airpuffs specifically applied to the dorsal body region seem to predominantly activate parvOT neurons. In a second step, we labeled parvOT neurons retrogradely by injecting the canine adenovirus serotype 2 (CAV2-Cre)[24] into the SON, and concomitantly injected the Cre-responder rAAV-expressing mCherry under the control of the OT promoter into the PVNs. In line with our previous results, airpuffs induced *c-fos* expression exclusively in retrogradely labeled mCherry-positive OT neurons (average 47.6%, 7.5 ± 3 neurons per PVN per hemisphere, $n = 4$; Fig. 2d and Supplementary Table 1b).

To explore the role of parvOT neurons in social interaction and their response to gentle non-nociceptive mechanical stimuli (airpuffs), we chose to manipulate their activity via virally expressed, designer receptors exclusively activated by designer drugs (DREADDs). To this end, we used a similar Cre-dependent viral-based strategy employing OTp-DIO-hM4D(Gi)-mCherry and OTp-DIO-hM3D(Gq)-mCherry rAAVs (Fig. 2e,f). As a first step, we verified the efficiency of DREADDs in modulating of parvOT neuron activity ex vivo, showing that hM3D(Gq)-CNO-induced parvOT activation significantly increased the spontaneous action potential (AP) frequency (baseline 0.85 ± 0.39 Hz versus clozapine *N*-oxide (CNO) 1.31 ± 0.51 Hz, $n = 9$; $P = 0.0039$; Extended Data Fig. 5a–c) and the number of evoked APs (16.18 ± 3.89 APs versus CNO 22.55 ± 5.66 APs, $n = 11$; $P = 0.0314$; Extended Data Fig. 5d–f). Consistent with this, hM4D(Gi)-CNO-induced inhibition (10 µM, 6 min) significantly decreased both the spontaneous AP frequency (baseline 1.38 ± 0.38 Hz versus CNO 0.36 ± 0.18 Hz, $n = 7$; $P = 0.0469$; Extended Data Fig. 5g–i) and the number of evoked APs (baseline 13 ± 2.02 APs versus CNO 7.75 ± 2.03 APs, $n = 11$; $P = 0.0007$; Extended Data Fig. 5j–l).

After the ex vivo results, we next performed in vivo recording in anesthetized animals to better understand the airpuff-induced activation of parvOT. For this purpose, PVN parvOT activity was imaged using the GCaMP6s reporter and fiber photometry[25] (Fig. 2e–h). Then, rats were injected with the DREADD ligand CNO (3 mg kg^{-1} intraperitoneally) and OT neuron Ca^{2+} transients were analyzed. Chemogenetic activation of the parvOT neurons enhanced the Ca^{2+} response to airpuffs (45 ± 9% increase of area under the curve (AUC; $P = 0.03$; Fig. 2i). Conversely, chemogenetic inhibition of the parvOT neurons reduced the response to airpuffs (65 ± 5% decrease of AUC; $P = 0.009$ compared with control; Fig. 2j).

Thus, we concluded that gentle non-nociceptive mechanical stimulation of the dorsal region activates parvOT neurons, which we hypothesized may drive the activity of the larger population of magnOT neurons.

Intra-PVN connectivity of parvOT and magnOT neurons. To validate this hypothesis, we first looked for direct synaptic contact of parvOT neurons on to magnOT somata and/or dendrites via injection of OTp-DIO-GFP rAAV into the PVN and Cav2-Cre into the SON to specifically label parvOT neurons (Extended Data Fig. 6a,b) in analogy to a previous study[13]. For three-dimensional (3D) reconstruction of interposition between axons of parvOT neurons and somatodendritic domains of magnOT neurons, we employed the IMARIS technique[26,27]. This approach allows precise identification of the location of synaptic contact by quantifying overlap with SYN-immunoreactive puncta. By performing IMARIS-assisted Sholl analysis, we found synaptic-like contacts of parvOT neurons with magnOT somata and dendrites (Fig. 3a and Extended Data Fig. 6; 6 dendritic contacts, 124 somatic contacts, $n = 354$) as well as an average chance of innervation of 34.9% (Fig. 3b), indicating that approximately a third of PVN magnOT neurons receive parvOT input. Based on these anatomical observations, we performed patch-clamp recording for functional validation of parvOT–magnOT neuron connection via rAAV-OTp-DIO-ChR2-mCherry (to label specifically parvOT) and rAAV-OTp-Venus (to label all OT neurons) injected into the PVN and Cav2-Cre injected into the SON (Fig. 3g). First, we confirmed the magnOT nature of recorded neurons through the presence of a hyperpolarizing transient outward rectification, as well as a weak low-threshold depolarization (Fig. 3h), by comparison to the electrophysiological properties of identified parvOT neurons (Fig. 3c–f). We observed that stimulation of parvOT neurons evoked responses in 45% of recorded magnOT neurons (9 of 20; Fig. 3i) with a significant increase in postsynaptic current (PSC) frequencies (baseline 0.158 ± 0.055 Hz versus ChR2 0.346 ± 0.15 Hz, $n = 9$; $P < 0.01$; Fig. 3i). Next, we aimed to visualize Ca^{2+} variations in magnOT neurons on DREADD-mediated activation of parvOT neurons via rAAV-OTp-DIO-hM3D(Gq)-mCherry and rAAV-OTp-GCaMP6s injected into the PVN and Cav2-Cre into the SON (Fig. 4a–d). After application of CNO (10 µM, 1 min), we observed that 40 ± 8% of recorded magnOT neurons responded to parvOT hM3D(Gq) stimulation, again confirming described

Fig. 2 | Gentle non-nociceptive mechanical stimuli trigger OT neuron activation. a, Head-fixed rats injected with rAAV-pOT-ChR2-mCherry were stimulated with airpuffs at anterior, central and posterior portions of the dorsal body region, whereas OT neurons were recorded with an opto-electrode. Top: PSTH example of OT neuron responses to airpuffs. Bottom: normalized PSTHs of 10 (of 23) recorded OT neuron responses to airpuffs in three dorsal body regions ((i) anterior; (ii) central; (iii) posterior); red indicates high spiking activity. ITR, inverted terminal repeat; NS, not significant. **b**, Top: statistics of average firing rate of OT neuron responses to airpuff stimulations (peak versus baseline, $^*P = 0.017$, $^{**}P = 0.025$, $^{***}P = 0.021$; $n = 23$ cells from 8 rats; one-way ANOVA followed by Bonferroni's post hoc comparison) indicates a significant increase above basal rate (dashed line). Bottom: latency of OT neuron responses to airpuffs. All data shown as average ± s.e.m. **c**, Fluorogold-injected rats received continuous airpuffs for 10 min and were killed and perfusion-fixed 90 min later. PVN slices were triple stained with antibodies against OT (blue), Fluorogold (red) and *c-fos* (green). The confocal image shows a Fluorogold-negative parvocellular OT neuron expressing *c-fos* (1 of 99 such double-labeled neurons observed in 4 rats). Scale bars, 100 and 10 µm (inset). **d**, Rats injected bilaterally with CAV2-Cre into the SON and rAAV-OTp-DIO-mCherry into the PVN were exposed to airpuffs for 10 min and killed 90 min later. The confocal image shows *c-fos* expression in a parvOT neuron (mCherry-positive, labeled via the retrograde CAV2-Cre, and is 1 of 60 such triple-labeled neurons observed in 4 rats). Scale bars, 100 and 10 µm (inset). **e**,**f**, Viral vectors for recording Ca^{2+} signals in GCaMP6s-expressing OT neurons during chemogenetic activation (**e**) or silencing (**f**) of parvocellular OT neurons. **g**,**h**, Examples of fiber photometry-based Ca^{2+} signals of PVN OT neuron population during airpuff stimulation (orange bars). Top: response to airpuffs 30–60 min after saline injection (control); bottom: response to airpuffs 30–60 min after CNO-induced activation (**g**) or silencing (**h**) of parvOT neurons. **i**, Average traces of Ca^{2+} responses to airpuffs 30–60 min after injection of either CNO to activate (Gq) parvOT neurons or saline (control). Each graphic is the average of 33 airpuff responses (11 airpuffs per animal, $n = 3$; AUC 0–30 s after airpuffs, relative to control; $^*P = 0.03$, paired, two-sided Student's *t*-test). **j**, Average traces of Ca^{2+} responses to airpuffs 30–60 min after injection of either CNO to silence (Gi) parvOT neurons or saline (control). Each graphic is the average of 33 airpuff responses (11 airpuffs per animal, $n = 3$; AUC 0–30 s after airpuffs, relative to control; $^{**}P = 0.007$, paired, two-sided Student's *t*-test). All data show average ± s.e.m.

anatomical connectivity (Figs. 3b,i and 4d). In responsive neurons, the number of Ca^{2+} transients was significantly increased, a result mirrored by the increase of AUCs (Fig. 4d). However, the width of these Ca^{2+} transients did not show any significant change, indicating that parvOT-induced magnOT activity does not trigger long-lasting Ca^{2+} transients, but several bursts of sharp Ca^{2+} peaks, as observed

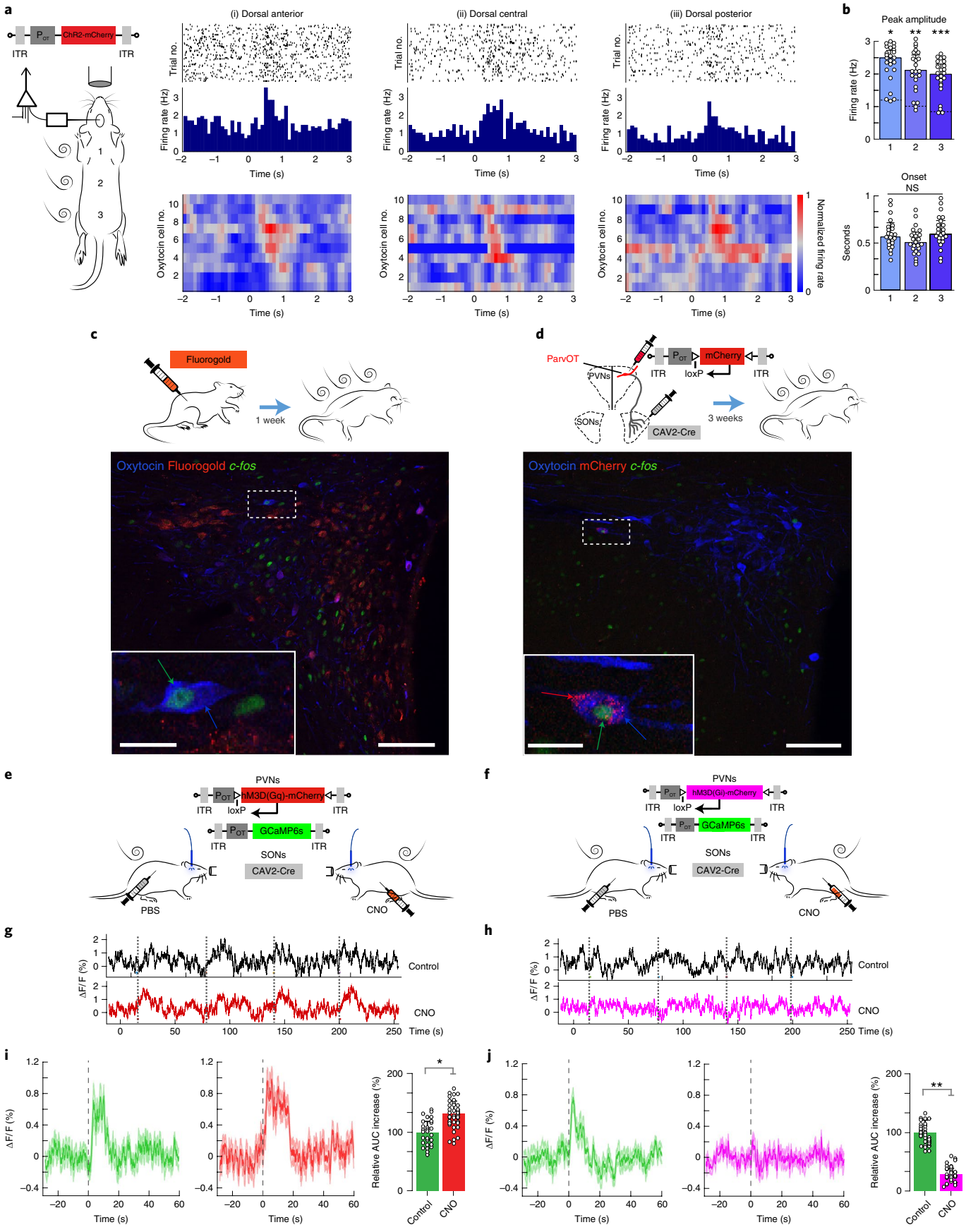

in the example traces (Fig. 4b). This feature was further confirmed by plotting the time course of Ca^{2+} event probability, showing that the probability of observing magnOT Ca^{2+} transients is increased over the 4 min after the ex vivo CNO treatment (Fig. 4c). These data indicate that parvOT neurons synapse on magnOT neurons within the PVN to drive their activity, as similarly reported for SON magnOT neurons in vivo[13].

Magnocellular neurons and their release of OT into blood, controlled by parvOT neurons. Using similar viral strategies, we expressed DREADDs—hM3D(Gq) or hM4D(Gi)—specifically in parvOT neurons and injected rAAV-OTp-GCaMP6s into the PVNs to express the Ca^{2+} indicator GCaMP6s in all PVN OT neurons (1,193 of 1,371 OT neurons expressed GCaMP6s, 87 ± 4%, $n = 4$; Fig. 4p). This allowed us to monitor the global activity of PVN OT neurons via fiber photometry in isoflurane-anesthetized rats on activation/inhibition of parvOT neurons. Activation of parvOT cells induced an increase in Ca^{2+} fluorescent signal of the PVN OT neuron population approximately 30 min after CNO injection (intraperitoneal 3 mg kg^{-1}) and lasting for >2 h (Fig. 4e–h). Conversely, inhibition of parvOT neurons decreased Ca^{2+} fluorescent signals of the general population 30 min after CNO injection and the effect lasted for more than 2 h (Fig. 4i–l). Administration of CNO did not have any effect on the Ca^{2+} signal in control animals lacking the DREADD receptors (Fig. 4m–o). Considering that the contribution of parvOT neurons to the OT population Ca^{2+} signal is negligible (Extended Data Fig. 7a–e), those results suggest that changes in parvOT neuron activity directly influence the firing pattern of large populations of PVN magnOT neurons. The similar kinetics of Ca^{2+} signal fluctuations after CNO activation of parvOT PVN neurons, together with airpuff application, were detected during recording of magnOT neurons in the SON, which do not contain parvOT neurons (Extended Data Fig. 7f–o).

To investigate whether parvOT-induced magnOT activity is followed by actual OT release, we analyzed neurohypophyseal OT release after chemogenetic activation of parvOT neurons. We performed blood sampling from the jugular vein before and after CNO injection (3 mg kg^{-1}; Fig. 4q) and found a significant increase in plasma OT 45 min ($P = 0.00093$ versus basal; $P = 0.0036$ versus OTp-mCherry control) and 90 min ($P = 0.002$ versus basal; $P = 0.0017$ versus OTp-mCherry control; Fig. 4r) after intraperitoneal CNO injections.

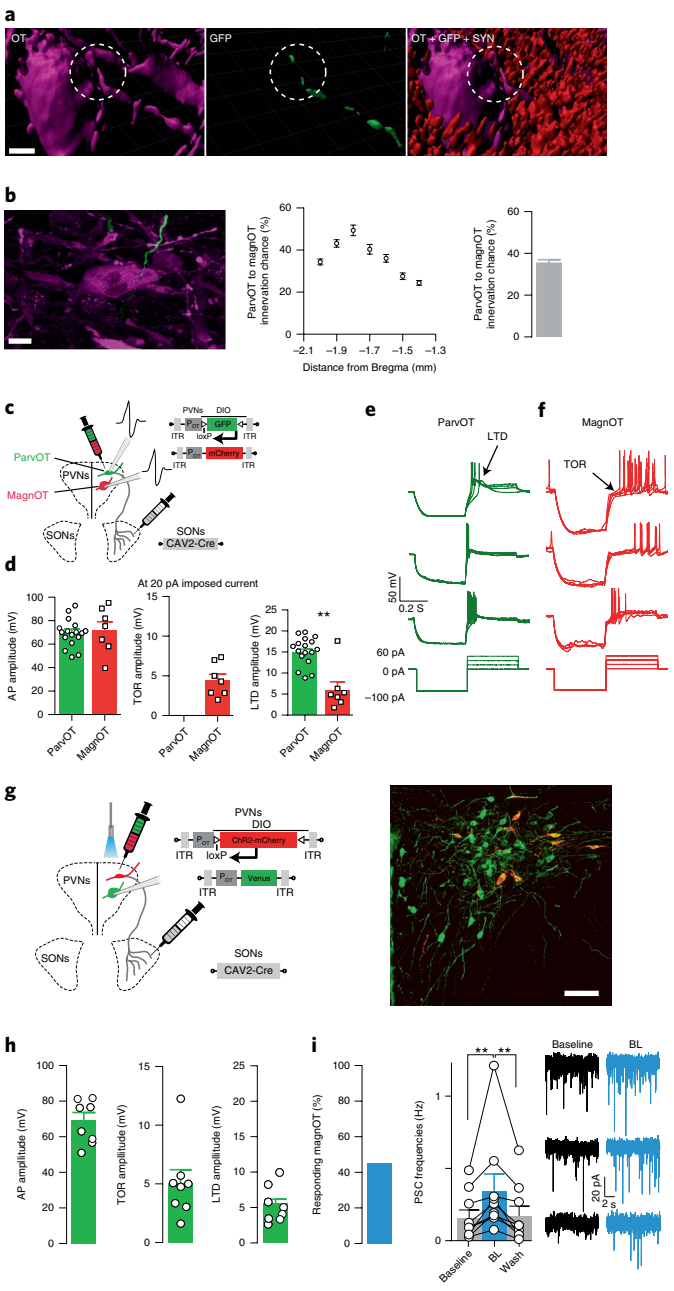

Fig. 3 | Intra-PVN connectivity of parvOT and magnOT neurons. a, Images show the 3D surface reconstruction of OT, GFP and SYN. Circles with dashed lines indicate the overlap of OT, GFP and SYN. Scale bar, 10 µm. **b**, Confocal image shows a single magnOT neuron (purple) innervated by a parvOT fiber (green). Scale bar, 10 µm. Dot-plot graph shows that the chance of innervation by parvOT neurons depends on the anatomical location of magnOT neurons within the PVN. Bar graph shows the average chance for magnOT PVN neurons to be innervated by parvOT axons ($n = 214$ cells from 3 rats). **c**, Schema of the viral injection into the SON and PVN plus the electrophysiological recording in the PVN (with pipette) for the recording of parvOT neurons (expressing mCherry + GFP) and magnOT neurons (expressing mCherry). **d**, Comparison of average and individual points of voltage amplitude between parvOT neurons ($n = 17$ cells from 4 rats) and magnOT neurons ($n = 7$ cells from 4 rats) for different electrophysiological parameters (AP; parvOT 70.12 ± 2.87 mV versus magnOT 71.65 ± 7.414 mV; $P = 0.82$, unpaired, two-sided Student's t-test; transient outward rectification (TOR): magnOT = 4.39 ± 0.79 mV; low threshold depolarization (LTD): parvOT 14.88 ± 0.81 mV versus magnOT 5.93 ± 1.98 mV; $^{**}P = 0.0019$, two-sided Mann–Whitney U-test). **e**, Example responses of three parvOT neurons to a hyperpolarizing current at −100 pA followed by four current injections starting from 0 to 60 pA. **f**, Example responses of three magnOT neurons to a hyperpolarizing current at −100 pA followed by four current injections starting from 0 pA to 60 pA. **g**, Left: schematic representation of viral vectors injected in the PVN (OTp-DIO-ChR2-mCherry and OTp-Venus) and the SON (CAV2-Cre) to transduce the expression of ChR2-mCherry in parvOT neurons and of Venus in PVN OT neurons. Right: image showing viral expression in the PVN in one of four rats. Scale bar, 100 µm. **h**, Average and individual points of voltage amplitude of magnOT neurons ($n = 8$ cells from 4 rats) for different electrophysiological parameters: AP, TOR and LTD. **i**, Average percentage (45%) of responding magnOT neurons ($n = 9$ cells) in all the magnOT neurons that have been recorded ($n = 20$ cells from 4 rats). MagnOT PSC frequency reversibly increases after parvOT ChR2 photostimulation ($n = 9$ cells). Example responses of three magnOT neurons in voltage clamp configuration at −70 mV before and after the ChR2 optogenetic stimulation of parvOT neurons. Baseline versus BL: $^{**}P < 0.001$; baseline versus wash: $^{**}P < 0.001$, Friedman's test followed by Dunn's post hoc test. BL, blue light. All data are represented as mean + s.e.m.

Taken collectively, these results indicate that parvOT neurons tightly control magnOT neuron activity in vivo to regulate peripheral OT release.

Differential neural inputs to parvOT and PVN magnOT neurons. These findings suggest that parvOT neurons act as 'first responders to somatosensory input', conveying information to the rest of the PVN OT neuronal population (that is, magnOT neurons). Hence, we asked whether parvOT neurons receive more synaptic inputs than magnOT ones in the PVN. In an attempt to assess potential differences of synaptic inputs to parvOT and magnOT neurons, we used IMARIS to quantify the total amount of SYN fluorescence at somata and dendrites. To perform an unbiased analysis, we created spheres that precisely engulfed magnOT and parvOT somata and accounted for individual variances in cell roundness and surface area (Methods). We found statistically significant differences at both the soma (Fig. 5a) and dendritic locations (Fig. 5b, at two different locations, 5 and 20 µm from the soma) and analyzed a total of 104 neurons (parvOT = 56, magnOT = 48), suggesting that parvOT neurons might receive more overall synaptic input.

Next, to uncover the origin of synaptic inputs to parvOT and magnOT neurons, we employed the retrograde trans-synaptic, EnvA-pseudotyped, G-deletion-mutant rabies virus (Rb-GFP[28]). To specifically distinguish inputs to parvOT and magnOT neurons, we used a double-conditional approach, which allows retrotracing of inputs to OT neurons that project to an area of choice (SON for parvOT and posterior pituitary for magnOT) (Methods; Fig. 5c,e).

In both groups of rats, we found green fluorescent protein (GFP)-expressing neurons in numerous brain regions, including the septum, medial preoptic area and amygdala (Fig. 5d,f and Extended Data Fig. 8h), demonstrating that parvOT and magnOT neurons receive a large number of common inputs (Supplementary Table 2). However, we detected the presence of GFP neurons in the paraventricular nucleus of thalamus, insula and habenula only after infection of parvOT neurons (Extended Data Fig. 8i), whereas GFP neurons in the substantia nigra were found only after primary infection of magnOT neurons (Extended Data Fig. 8j). In line with the IMARIS analysis, the total number of neurons projecting to parvOT and magnOT neurons was 1,963.6 ± 710 and 694.8 ± 121 neurons, respectively ($P = 0.02$; Fig. 5g). Although we did not find between-group differences in the proportion of inputs coming from hypothalamic and extrahypothalamic areas (Fig. 5h), the periqueductal gray and subfornical organ showed preferential innervation of parvOT and magnOT neurons, respectively (Fig. 5i). This indicates that parvOT neurons receive at least partially distinct, and more pronounced neuronal inputs than magnOT neurons.

ParvOT neurons modulate social behavior. To test whether this small population of parvOT neurons can modulate social behavior by their effects on the activity of the much more abundant magnOT neurons, we used the previously described chemogenetic approach to silence or activate them during behavioral tests (Fig. 6a). Then 3 weeks after viral injection, rats were injected intraperitoneally with either CNO (3 mg kg^{-1}) or saline 60 min before social interaction tests (Fig. 6b). Selective inhibition of the parvOT neurons resulted in less social interaction: in the FSI test, the time spent with a conspecific was reduced by 37 ± 6 s (over 5-min sessions, $P < 0.001$; Supplementary Video 2). By contrast, in the CSI test, where no physical contact is allowed, the time spent by the experimental rat approaching the stimulus rat was unchanged (Fig. 6c–e; $n = 15$ rats). Conversely, CNO-induced activation of parvOT neurons led to more social interaction: in the FSI test, the time spent with a conspecific increased

Fig. 4 | Magnocellular neurons and their release of OT into blood are controlled by parvOT neurons. a, To allow the expression of hM3D(Gq) on parvOT PVN to SON projecting neurons, rats' SON are infected with a CAV2-Cre rAAV and the PVN are infected with an AAV, allowing the Cre-dependent expression of hM3D(Gq) under the control of the OT promoter. We also make PVN OT neurons express the calcium indicator GCaMP6s to monitor calcium transients in parvOT neurons. **b**, Example traces of the effect of CNO (10 µM, 6 min) on PVN oxytocinergic neuron calcium activity. **c**, CNO application increases the number of calcium transients by 5-fold ± 1-fold (solid line: average, shaded area: s.e.m., $P = 0.0019$, Wilcoxon's test) and the AUC by 15- ± 9-fold ($P = 0.0043$, Wilcoxon's test) in 40 ± 8% of recorded magnOT neurons ($n = 20$ slices from 7 rats, 70 cells). **d**, Calcium event probability, fraction of responses, number of peaks, AUC and peak duration of calcium events in PVN OT neurons. After CNO application, the probability of observing a calcium peak is increased over ~4 min, but the duration of those peaks remains unchanged (ratio = 2 ± 0.7, $P = 0.46$, paired, two-sided Student's t-test). Bar plots show mean ± s.e.m. **e**–**h**, Schema of viral vectors injected and implanted optic fiber-for-fiber photometry recording (**e**) of PVN OT neurons with concomitant DREADD-Gq activation of parvOT neurons. Example traces (**f**) of recorded GCaMP6s signal from PVN OT neurons before and after CNO-induced activation of parvOT neurons. Normalized AUC of GCaMP6s signal (**g**, solid line: average, shaded area: s.e.m., 1-min bin size) of PVN OT neurons showing increase of cellular activity after parvOT activation mediated by CNO intraperitoneal injection (indicated by arrow). The 30-min averaged AUC (**h**) showing a gradual increase of cellular activity (baseline AUC versus 0–30 min, $P = 0.0606$, versus 30–60 min, $^{*}P = 0.0403$) that lasts at least 120 min (baseline AUC versus 60–90 min, $^{*}P = 0.028$; versus 90–120 min, $^{*}P = 0.0325$, $n = 6$ rats, two-way ANOVA and Tukey's corrected post hoc comparison). **i**–**l**, Schema of viral vectors injected and implanted optic fiber for fiber photometry recording (**i**) of PVN OT neurons with concomitant DREADD-Gi inhibition of parvOT neurons. Example traces (**j**) of recorded GCaMP6s signal from PVN OT neurons before and after CNO-induced inhibition of parvOT neurons. Normalized AUC of GCaMP6s signal (**k**, solid line: average, shaded area: s.e.m., 1-min bin size) of PVN OT neurons showing decrease of cellular activity after parvOT inhibition mediated by intraperitoneal CNO injection (indicated by arrow). The 30-min averaged AUC (**l**) showing a gradual decrease of cellular activity (baseline AUC versus 0–30 min, $P = 0.058$, versus 30–60 min, $^{***}P = 0.00013$) that lasts at least 120 min (baseline AUC versus 60–90 min, 90–120 min, $^{***}P = 0.00019$, $n = 3$ rats, two-way ANOVA and Tukey's corrected post hoc comparison). **m**–**o**, Schema of viral vectors injected and implanted optic fiber-for-fiber photometry recording (**m**) of PVN OT neurons in control animals (DREADD free) expressing GFP in parvOT neurons. Normalized AUC of GCaMP6s signal (**n**, solid line: average, shaded area: s.e.m., 1-min bin size) of PVN OT neurons showing no significant changes in Ca^{2+} signal on CNO injection. No significant changes are detected in 30-min averaged AUC (**o**) up to 120 min ($P = 0.109$, $n = 2$ rats, two-way ANOVA and Tukey's corrected post hoc comparison). **p**, Panels of immunostained section of the PVN showing post hoc verification of implanted optic fiber above the PVN and co-localization of immunoreactive GCaMP6s (green, top left), DIO-hM3D(Gq)-mCherry (red, bottom left) and OT (blue, right) in one of six rats. Arrows indicate mCherry-positive parvOT neurons. Scale bars, 100 µm and 10 µm (inset). **q**, Schema of viral vectors injected for DREADD-Gq activation of parvOT neurons and blood sampling from the jugular vein. **r**, Chemogenetic activation of parvOT neurons evokes peripheral OT release. Plasma OT (pg ml^{-1}) taken under basal conditions and 45 and 90 min after intraperitoneal CNO (3 mg kg^{-1}; depicted by arrow; $n = 8$ rats parvOT Gq group, $n = 6$ rats control group). At 45 min, $^{++}P = 0.00093$ versus basal (−45 min), $^{**}P = 0.0036$ versus control (OTp-mCherry) and, at 90 min, $^{++}P = 0.002$ versus basal, $^{**}P = 0.0017$ versus control. Two-way repeated-measures ANOVA with Bonferroni post hoc correction. Data are presented as mean ± s.e.m.

by 10±6 s (P=0.04). In the CSI test, no significant difference in approaching time was measured between saline- and CNO-injected rats (Fig. 6f–h; n=9 rats).

Inhibition and activation of parvOT neurons also had opposite effects on crawling behavior (Fig. 6e,h). Moreover, after inhibiting parvocellular OT neurons, rats often actively avoided

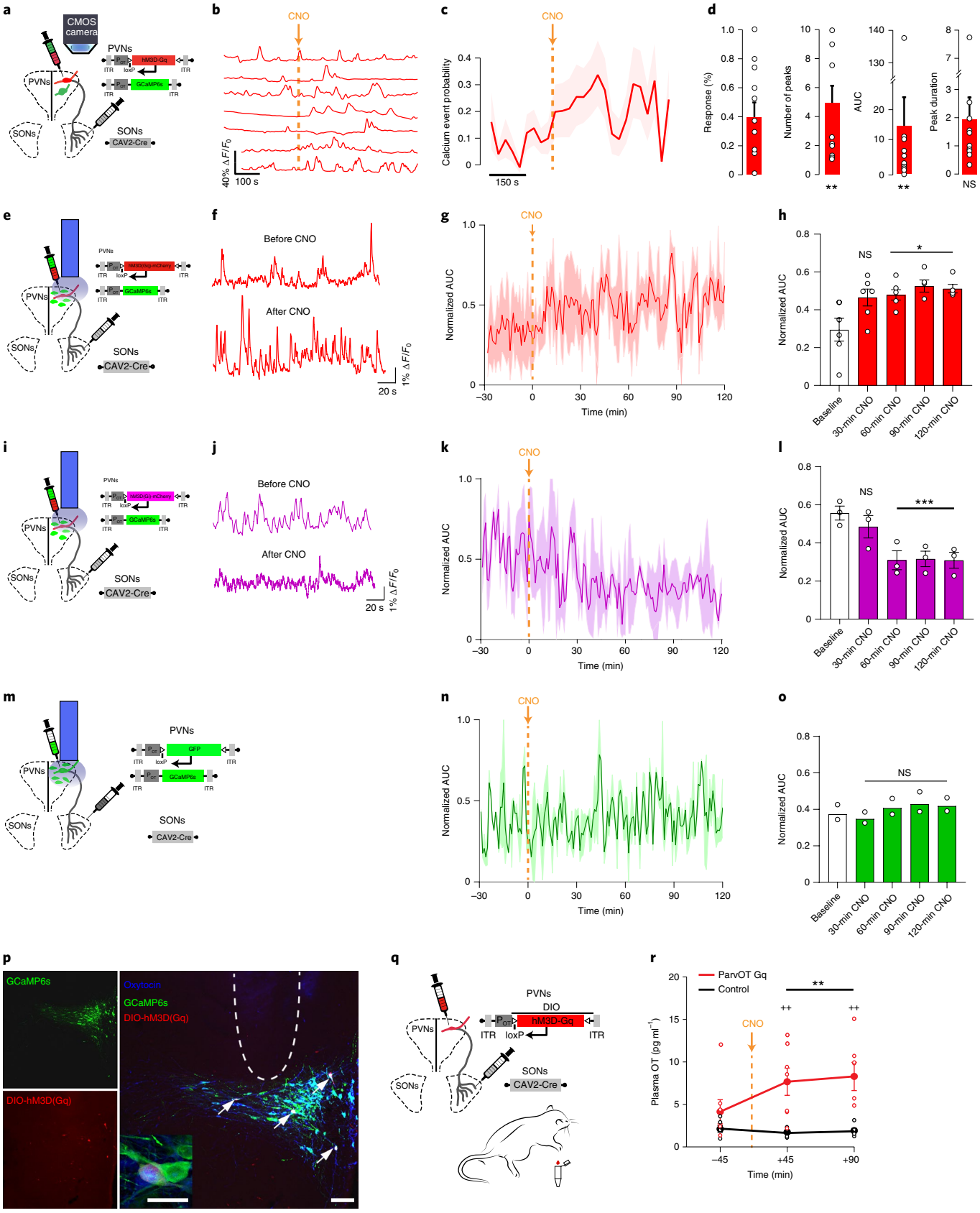

the stimulus rat, a behavior never observed in the control group (Extended Data Fig. 9c). Control rats injected with control virus rAAV-OTp-DIO-GFP receiving saline or CNO showed no behavioral differences (Extended Data Fig. 9a).

To show that alterations of social behaviors induced by DREADD-based manipulation of parvOT neuron activity were indeed an effect mediated by central OT release, the parvOT activation (Gq) experiment was repeated while applying an OTR antagonist[29] by intracerebroventricular infusion (0.75 µg per 5 µl)[30]. Compared with saline-infused control animals, OTR antagonist-infused animals showed a strong reduction in social interactions (37 ± 18% reduction, $P = 0.007$, $n = 12$ rats), regardless of CNO administration, whereas, without OTR antagonist, CNO application caused increased social interactions (16 ± 3% increase, $P = 0.04$, $n = 12$; Fig. 6i and Extended Data Fig. 9h). We did not observe a CNO- or OTR antagonist-induced effect on locomotor activity (Extended Data Fig. 9b,d–e). This result confirms that the downstream effect on CNO-induced activation of parvOT neurons of social behavior is indeed mediated by OT and its receptors. In a second group of rats ($n = 10$) expressing GFP in parvOT neurons, administration of an OTR antagonist also had a comparable effect in reducing social behavior; as expected, CNO itself did not have any effect on social interaction of animals (Fig. 6j and Extended Data Fig. 9i).

Discussion

In the present study, we provide evidence that somatosensory stimulation in female rats activates parvOT neurons, which subsequently drive the activation of the much larger population of magnOT neurons. Using ex vivo and in vivo approaches, we demonstrated that parvOT neurons synapse on magnOT neurons to elicit a central effect of OT to promote interfemale communication.

Social touch evokes OT neuronal activity. The use of single-unit in vivo recording precludes discrimination between parvOT and magnOT neurons. However, considering the limited number of parvOT neurons (~30 parvOT cells[13] versus ~1,200 magnOT cells[31] in the PVN of each hemisphere), it is highly likely that we exclusively recorded from magnOT cells. In support, we found that nonaggressive social interactions of female rats and, in particular, physical contacts elicited a coordinated, clustered spiking activity of PVN OT neurons—a pattern that strongly facilitates activity-dependent secretion of OT from nerve terminals of magnOT cells in the pituitary[17] (Extended Data Fig. 2h–j). This activity is almost synchronous across recorded OT neurons, and is highly correlated with theta rhythmicity of PVN local field potentials. These coordinated changes in OT neuronal electrical activity occurred only during FSI, allowing physical contacts between conspecifics, but not during CSI, where physical touch between animals was prevented by a barrier. Moreover, detailed analysis of PVN OT neuron activity during social behaviors revealed that the highest increase in neuronal firing occurred immediately after (0–10 s) crawling on top or being crawled behaviors (Fig. 1), that is, social contacts involving activation of cutaneous sensory nerves.

To test whether non-noxious repetitive somatosensory stimulations directly influence PVN OT neuron activity, even in the absence of other stimuli, we applied airpuff stimulations to the skin of the dorsal area of the rat, in lightly anesthetized conditions, while measuring action potentials of PVN neurons. Notably, airpuffs induced a significant increase in spiking activity of most (83%) recorded putative magnOT neurons, but had little or no effect on the activity of non-OT PVN neurons, reinforcing the idea that somatosensory inputs selectively activate magnOT neurons. This finding is in line with previous studies[32] that reported increased OT plasma levels in rats after 10 min of massage-like stroking. Furthermore, the stimulation of low-threshold mechanoreceptors, particularly the touch-sensitive nerve fiber C-tactile afferents is known to trigger OT release, and has been associated with increased social motivation in rodents and humans[33].

ParvOT neurons control PVN magnOT neuron activity. To shed light on the causal link between somatosensory stimulation and social behavior, we focused our research on a specific subtype of 'parvocellular' OT neurons. These neurons communicate with various autonomic centers in the brain stem and spinal cord[20], and are involved in analgesia during acute pain[13].

When we applied low-intensity, non-noxious cutaneous stimulation (airpuff) in awake rats, we observed a sustained increase of *c-fos* expression in parvOT neurons in the PVN (Fig. 2). Of note, we found that airpuffs induced *c-fos* expression in parvOT, but not in magnOT, neurons. However, the absence of *c-fos* expression in magnOT cells does not necessarily indicate the absence of their increasing activity[34–36]. Indeed, only dramatic physiological challenges such as hemorrhage, salt loading or fear evoke *c-fos* expression in magnOT neurons[34,37]. Importantly, during lactation magnOT neurons release a large amount of OT into the peripheral circulation although an increase in *c-fos* expression was never found. In analogy, our findings demonstrate increased OT plasma concentrations after chemogenetic activation of parvOT neurons (Fig. 4) via a demonstrated parvOT → magnOT connectivity, although without detectable *c-fos* immunosignal in magnOT neurons releasing the neuropeptide into the blood.

Furthermore, chemogenetic activation or inhibition of parvOT neurons via DREADDs resulted, respectively, in an increase or decrease in OT neuron activity in response to the airpuff stimulation (Fig. 2). This suggests that parvOT neurons can be activated by both nociceptive[13] and non-nociceptive stimuli (in the present study) and subsequently promote analgesia as well as social behavior. Such pleotropic effects of OT originating from the same parvOT neurons require further investigation.

To provide additional evidence that parvOT neurons modulate magnOT neuron activity within the PVN, we employed a

Fig. 5 | ParvOT neurons receive more inputs than magnOT neurons. a, Three-dimensional reconstruction of parvOT and magnOT neurons and the quantification of SYN fluorescence. Asterisks (white) indicate the placement of the spheres (yellow) used to quantify the total amount of SYN fluorescence (red). Top: the placement of a sphere around a magnOT neuron soma; bottom: the placement of a sphere on to a parvOT neuron dendrite. Scale bars, 5 µm. **b**, Quantification of SYN fluorescence in close proximity to parvOT ($n = 56$ cells from 3 rats) and magnOT ($n = 48$ cells from 3 rats) neurons at somatic (top) and dendritic locations (bottom) considering differences in cellular roundness and surface area (adjusted) (unpaired, two-sided Student's *t*-test, $^{***}P < 0.0001$). **c**,**e**, Virus injection strategy to retrotrace inputs from parvOT (**c**) and magnOT (**e**) neurons, respectively. **d**,**f**, Schema representing the proportion of inputs (number of inputs from one brain area/total number of inputs) from each brain area to parvOT (**d**) and magnOT (**f**) neurons, respectively. Brain areas projecting only to parvOT or magnOT neurons are circled in green or purple, respectively. See Supplementary Table 2 for a full list of abbreviations for structures in **d** and **f**. **g**, Quantification of the total number of inputs to parvOT and magnOT neurons (two-sided Student's *t*-test, $^{*}P = 0.0223$, $n = 5$ rats per group). **h**, Proportion of inputs to parvOT and magnOT neurons located in or outside the hypothalamus. Numbers indicate average number of neurons. **i**, Bar graphs showing the proportion of inputs coming from brain areas that show preferential innervation of parvOT or magnOT neurons. Two-sided Student's *t*-test; asterisks indicate significant difference: $^{*}P = 0.0315$, $^{**}P = 0.0153$, $^{***}P = 0.0264$, $^{****}P = 0.0299$, $^{*****}P = 0.0453$ and $^{******}P = 0.0011$; $n = 5$ rats per group. Data represented as mean ± s.e.m.

combination of immunohistochemistry and 3D anatomical reconstruction. We found 1.5- to 4-fold more synaptic-like contacts on parvOT somata and dendrites compared with the respective compartments of magnOT neurons (Fig. 5). This finding is supported by retrograde tracing data, which demonstrate substantially more inputs to parvOT neurons than to magnOT neurons (Fig. 5).

Do parvOT neurons control social behavior?. To investigate how parvOT neurons modulate social behavior, we performed chemogenetic manipulation of parvOT neurons by viral means. We found that targeted activation or inhibition of parvOT neurons increased or decreased the total time of social interaction with a conspecific, respectively. Furthermore, the intracerebroventricular

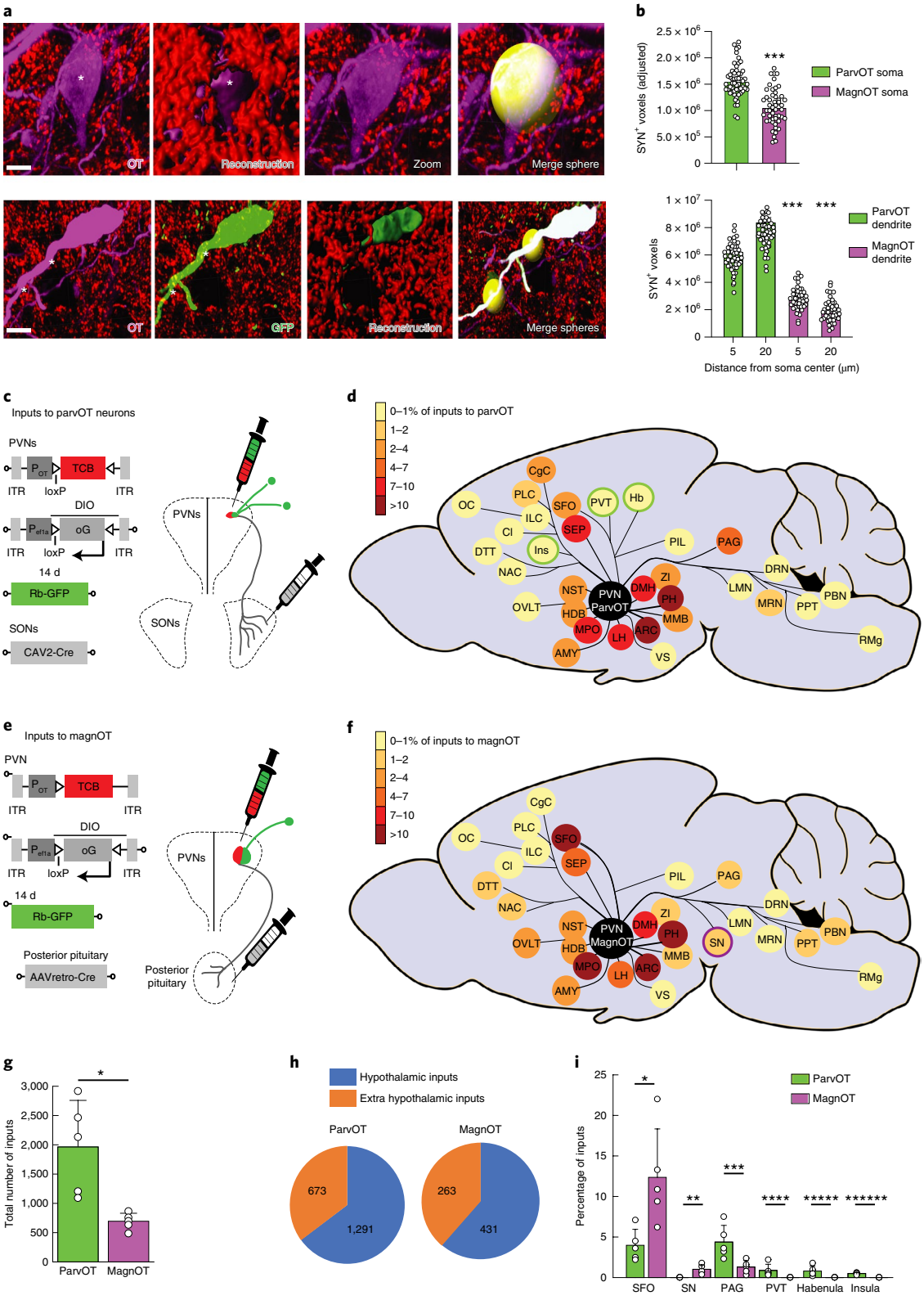

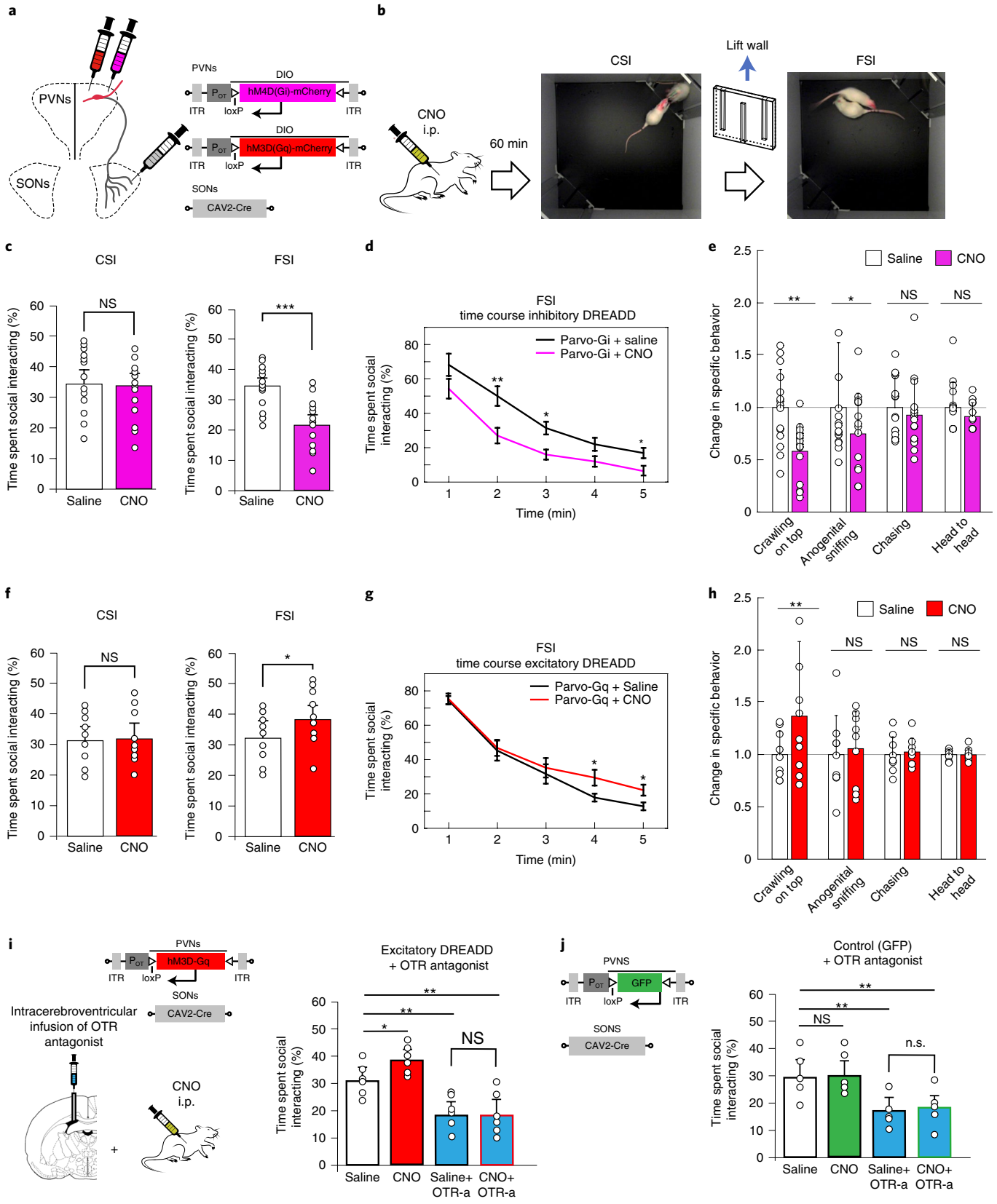

application of an OTR antagonist prevented CNO-induced social interaction after chemogenetic activation of parvOT neurons (Fig. 6). This suggests that the excitation of parvOT neurons is transmitted to magnOT cells, which, in turn, project axonal collaterals to numerous forebrain regions[5,7]. Given that parvOT neurons exclusively project to the brain stem and spinal cord[38], our results allow the hypothesis that the OTR antagonist blocks the action of OT released from magnOT axons in socially relevant brain regions, resulting in the attenuation of social communication between female conspecifics.

Fig. 6 | Modulation of parvocellular OT neurons alters social behavior. a, Viral vectors used to express genes of interest (hM4D(Gi)-mCherry or hM3D(Gq)-mCherry) in parvOT neurons. **b**, CNO or saline was injected intraperitoneally (i.p.) 60 min before the behavioral tests. **c**, Silencing parvOT neurons (Parvo-Gi group): percentage of time spent by an experimental rat injected with saline or CNO socially interacting with a conspecific in CSI ($P=0.41$) and FSI ($n=15$ rats, $^{***}P=0.0001$, paired, two-sided Student's t-test), calculated over the 5-min session. **d**, Temporal dynamics of time spent in social interaction in 1-min bins (second minute, $^{**}P=0.01$; third minute $^{*}P=0.03$; fifth minute $^{*}P=0.04$; $n=15$ rats, two-way ANOVA time × treatment). **e**, Parvo-Gi group: time spent in different social behaviors in rats injected with saline or CNO: crawling on top ($^{**}P=0.008$), sniffing ($^{*}P=0.012$), chasing ($P=0.13$), head to head ($P=0.31$) ($n=15$ rats, one-way ANOVA, Tukey's corrected post hoc comparison). **f**, Activation of parvOT neurons (Parvo-Gq group): average time spent in social interaction with conspecific stimulus in CSI ($P=0.32$) and FSI ($n=9$ rats, $^{*}P=0.04$, paired, two-sided Student's t-test) after CNO or saline injection. **g**, Temporal dynamics of time spent in social interaction in 1-min bins for rats injected with CNO or saline (fourth minute, $P=0.03$; fifth minute, $n=9$ rats, $P=0.05$, two-way ANOVA time × treatment). **h**, Parvo-Gq group: time spent in different social behaviors in rats injected with saline or CNO: mounting ($^{**}P=0.006$), sniffing ($P=0.44$), chasing ($P=0.27$), head to head ($P=0.11$) ($n=9$ rats, one-way ANOVA, Tukey's corrected post hoc comparison). **i**, OTR antagonist intracerebroventricular infusion decreases social interaction even in the presence of pharmacological activation (hM3D-Gq) of parvOT neurons. Percentage of social interaction time is shown in different conditions: saline (control), CNO, OTR antagonist (OTR-a) or CNO + OTR antagonist administration. Time spent social interacting over 5-min sessions. Saline intraperitoneally and intracerebroventricularly: 90 ± 19 s; CNO intraperitoneally and saline intracerebroventricularly: 105 ± 15 s, $^{*}P=0.04$, $n=6$ rats; saline intraperitoneally and OTR antagonist intracerebroventricularly: 54 ± 17 s, $^{**}P=0.007$; CNO intraperitoneally and OTR antagonist intracerebroventricularly: 56 ± 16 s, $^{**}P=0.009$, $n=6$ rats (one-way ANOVA and Tukey's corrected post hoc comparison). **j**, Control group in which parvOT neurons express GFP. Saline intraperitoneally and intracerebroventricularly: 88 ± 18 s; CNO intraperitoneally and saline intracerebroventricularly: 89 ± 14 s, $n=5$ rats; saline intraperitoneally and OTR antagonist intracerebroventricularly: 53 ± 14 s, $^{**}P=0.008$; CNO intraperitoneally and OTR antagonist intracerebroventricularly: 57 ± 15 s, $^{**}P=0.001$, $n=5$ rats (one-way ANOVA and Tukey's corrected post hoc comparison). All data are represented as mean ± s.e.m.

A stable OT-mediated social interaction throughout female life?. Although we exclusively used virgin females in our present study, it will be important to investigate how pregnancy and lactation change the OT-dependent response to somatosensory stimulation. Given the drastic activation of the OT system and close physical contact with the offspring peripartum[39–41], it is plausible that the reward of tactile stimulation changes as well. Moreover, due to the interaction of OT and prolactin during the milk letdown reflex[42,43], the nipples might become more sensitive to the suckling of pups, which could translate into a more rewarding experience for mothers. Further studies are needed to assess the intricate interrelationship of social touch, social behavior and social motivation, which requires concomitant actions of OT, serotonin and dopamine within the nucleus accumbens and ventral tegmental area[22,44], in females as well as males. Accordingly, we found that parvOT, but not magnOT, neurons are innervated by neurons of the insular cortex, which is a critical region processing social touch[45], and could thus be potentially involved in the recruitment of the oxytocinergic system during social tactile stimulation.

Taken together, our data extend the current knowledge of the interrelationship of intracerebral OT release, social touch and its behavioral correlates. Our results suggest that parvOT neurons translate mechanosensory information from the periphery into social behavior (Extended Data Fig. 10), but the precise ascending pathways from cutaneous nerves—via the parvOT → magnOT circuit—to forebrain regions controlling social behaviors await further investigation.

Although intranasal OT application has improved clinical outcomes of schizophrenia, post-traumatic stress disorders and autism spectrum disorders, there is still an ongoing debate about the validity of these findings[46], suggesting that evoking endogenous OT release might be a more reliable way to exploit the benefits of this neuropeptide. Thus, a combination of gentle touch, social interaction and/or intranasal OT application might be a powerful tool to treat human mental diseases, in which the OT system is compromised[47,48].

Online content

Any methods, additional references, Nature Research reporting summaries, extended data, supplementary information, acknowledgements, peer review information; details of author contributions and competing interests; and statements of data and code availability are available at https://doi.org/10.1038/s41593-020-0674-y.

Received: 10 January 2019; Accepted: 18 June 2020;
Published online: 27 July 2020

References

1. Lee, H.-J., Macbeth, A. H., Pagani, J. & Scott Young, W. 3rd. Oxytocin: the great facilitator of life. *Prog. Neurobiol.* **88**, 127–151 (2010).
2. Jurek, B. & Neumann, I. D. The oxytocin receptor: from intracellular signaling to behavior. *Physiol. Rev.* **98**, 1805–1908 (2018).
3. Walum, H. & Young, L. J. The neural mechanisms and circuitry of the pair bond. *Nat. Rev. Neurosci.* **19**, 643–654 (2018).
4. Russell, J. A., Leng, G. & Douglas, A. J. The magnocellular oxytocin system, the fount of maternity: adaptations in pregnancy. *Front. Neuroendocrinol.* **24**, 27–61 (2003).
5. Knobloch, H. S. et al. Evoked axonal oxytocin release in the central amygdala attenuates fear response. *Neuron* **73**, 553–566 (2012).
6. Marlin, B. J. & Froemke, R. C. Oxytocin modulation of neural circuits for social behavior. *Dev. Neurobiol.* **77**, 169–189 (2017).
7. Grinevich, V. & Stoop, R. Interplay between oxytocin and sensory systems in the orchestration of socio-emotional behaviors. *Neuron* **99**, 887–904 (2018).
8. Dumais, K. M., Alonso, A. G., Immormino, M. A., Bredewold, R. & Veenema, A. H. Involvement of the oxytocin system in the bed nucleus of the stria terminalis in the sex-specific regulation of social recognition. *Psychoneuroendocrinology* **64**, 79–88 (2016).
9. Dumais, K. M., Alonso, A. G., Bredewold, R. & Veenema, A. H. Role of the oxytocin system in amygdala subregions in the regulation of social interest in male and female rats. *Neuroscience* **330**, 138–149 (2016).
10. Resendez, S. L. et al. Social stimuli induce activation of oxytocin neurons within the paraventricular nucleus of the hypothalamus to promote social behavior in male mice. *J. Neurosci.* **40**, 2282–2295 (2020).
11. Bobrov, E., Wolfe, J., Rao, R. P. & Brecht, M. The representation of social facial touch in rat barrel cortex. *Curr. Biol.* **24**, 109–115 (2014).
12. Chen, P. & Hong, W. Neural circuit mechanisms of social behavior. *Neuron* **98**, 16–30 (2018).
13. Eliava, M. et al. A new population of parvocellular oxytocin neurons controlling magnocellular neuron activity and inflammatory pain processing. *Neuron* **89**, 1291–1304 (2016).
14. Lima, S. Q., Hromádka, T., Znamenskiy, P. & Zador, A. M. PINP: a new method of tagging neuronal populations for identification during in vivo electrophysiological recording. *PLoS ONE* **4**, e6099 (2009).
15. Leng, T., Leng, G. & MacGregor, D. J. Spike patterning in oxytocin neurons: capturing physiological behaviour with Hodgkin–Huxley and integrate-and-fire models. *PLoS ONE* **12**, e0180368 (2017).
16. Netser, S., Haskal, S., Magalnik, H. & Wagner, S. A novel system for tracking social preference dynamics in mice reveals sex- and strain-specific characteristics. *Mol. Autism* **8**, 53 (2017).
17. Maícas-Royo, J., Leng, G. & MacGregor, D. J. A predictive, quantitative model of spiking activity and stimulus-secretion coupling in oxytocin neurons. *Endocrinology* **159**, 1433–1452 (2018).
18. Portfors, C. V. Types and functions of ultrasonic vocalizations in laboratory rats and mice. *J. Am. Assoc. Lab. Anim. Sci.* **46**, 28–34 (2007).

19. Lenschow, C. et al. Sexually monomorphic maps and dimorphic responses in rat genital cortex. *Curr. Biol.* **26**, 106–113 (2016).
20. Althammer, F. & Grinevich, V. Diversity of oxytocin neurones: beyond magno- and parvocellular cell types? *J. Neuroendocrinol.* **30**, e12549 (2018).
21. Johnson, Z. V. et al. Central oxytocin receptors mediate mating-induced partner preferences and enhance correlated activation across forebrain nuclei in male prairie voles. *Horm. Behav.* **79**, 8–17 (2016).
22. Hung, L. W. et al. Gating of social reward by oxytocin in the ventral tegmental area. *Science* **357**, 1406–1411 (2017).
23. Okabe, S., Yoshida, M., Takayanagi, Y. & Onaka, T. Activation of hypothalamic oxytocin neurons following tactile stimuli in rats. *Neurosci. Lett.* **600**, 22–27 (2015).
24. Bru, T., Salinas, S. & Kremer, E. J. An update on canine adenovirus type 2 and its vectors. *Viruses* **2**, 2134–2153 (2010).
25. Gunaydin, L. A. et al. Natural neural projection dynamics underlying social behavior. *Cell* **157**, 1535–1551 (2014).
26. VanRyzin, J. W. et al. Microglial phagocytosis of newborn cells is induced by endocannabinoids and sculpts sex differences in juvenile rat social play. *Neuron* **102**, 435–449.e6 (2019).
27. Erny, D. et al. Host microbiota constantly control maturation and function of microglia in the CNS. *Nat. Neurosci.* **18**, 965–977 (2015).
28. Wickersham, I. R. et al. Monosynaptic restriction of transsynaptic tracing from single, genetically targeted neurons. *Neuron* **53**, 639–647 (2007).
29. Manning, M., Stoev, S., Cheng, L. L., Ching Wo, N. & Chan, W. Y. Design of oxytocin antagonists, which are more selective than atosiban. *J. Pept. Sci.* **7**, 449–465 (2001).
30. Grund, T. et al. Neuropeptide S activates paraventricular oxytocin neurons to induce anxiolysis. *J. Neurosci.* **37**, 12214–12225 (2017).
31. Rhodes, C. H., Morriell, J. I. & Pfaff, D. W. Immunohistochemical analysis of magnocellular elements in rat hypothalamus: Distribution and numbers of cells containing neurophysin, oxytocin, and vasopressin. *J. Comp. Neurol.* **198**, 45–64 (1981).
32. Uvnäs-Moberg, K., Handlin, L. & Petersson, M. Self-soothing behaviors with particular reference to oxytocin release induced by non-noxious sensory stimulation. *Front. Psychol.* **5**, 1529 (2015).
33. Walker, S. C., Trotter, P. D., Swaney, W. T., Marshall, A. & Mcglone, F. P. C-tactile afferents: Cutaneous mediators of oxytocin release during affiliative tactile interactions? *Neuropeptides* **64**, 27–38 (2017).
34. Brown, C. H., Bains, J. S., Ludwig, M. & Stern, J. E. Physiological regulation of magnocellular neurosecretory cell activity: integration of intrinsic, local and afferent mechanisms. *J. Neuroendocrinol.* **25**, 678–710 (2013).
35. Hoffman, G. E. & Lyo, D. Anatomical markers of activity in neuroendocrine systems: are we all 'Fos-ed out'? *J. Neuroendocrinol.* **14**, 259–268 (2002).
36. Hoffman, G. E., Smith, M. S. & Verbalis, J. G. c-Fos and related immediate early gene products as markers of activity in neuroendocrine systems. *Front. Neuroendocrinol.* **14**, 173–213 (1993).
37. Hasan, M. T. et al. A fear memory engram and its plasticity in the hypothalamic oxytocin system. *Neuron* **103**, 133–146.e8 (2019).
38. Stern, J. E. Electrophysiological and morphological properties of pre-autonomic neurones in the rat hypothalamic paraventricular nucleus. *J. Physiol.* **537**, 161–177 (2001).
39. Bosch, O. J. Brain oxytocin correlates with maternal aggression: link to anxiety. *J. Neurosci.* **25**, 6807–6815 (2005).
40. Fenelon, V. S., Poulain, D. A. & Theodosis, D. T. Fos synthesis and neuronal activation: analysis of Fos immunoreactivity in identified magnocellular neurons during lactation. *Ann. N.Y. Acad. Sci.* **689**, 508–511 (1993).
41. Neumann, I., Douglas, A. J., Pittman, Q. J., Russell, J. A. & Landgraf, R. Oxytocin released within the supraoptic nucleus of the rat brain by positive feedback action is involved in parturition-related events. *J. Neuroendocrinol.* **8**, 227–233 (1996).
42. Augustine, R. A. et al. Prolactin regulation of oxytocin neurone activity in pregnancy and lactation. *J. Physiol.* **595**, 3591–3605 (2017).
43. Kennett, J. E. & McKee, D. T. Oxytocin: an emerging regulator of prolactin secretion in the female rat. *J. Neuroendocrinol.* **24**, 403–412 (2012).
44. Dölen, G., Darvishzadeh, A., Huang, K. W. & Malenka, R. C. Social reward requires coordinated activity of nucleus accumbens oxytocin and serotonin. *Nature* **501**, 179–184 (2013).
45. McGlone, F., Wessberg, J. & Olausson, H. Discriminative and affective touch: sensing and feeling. *Neuron* **82**, 737–755 (2014).
46. Leng, G. & Ludwig, M. Reply to: Improving research standards to restore trust in intranasal oxytocin. *Biol. Psychiatry* **79**, e55–e56 (2016).
47. Meyer-Lindenberg, A., Domes, G., Kirsch, P. & Heinrichs, M. Oxytocin and vasopressin in the human brain: social neuropeptides for translational medicine. *Nat. Rev. Neurosci.* **12**, 524–538 (2011).
48. Grinevich, V. & Neumann, I. D. How puzzle stones from animal studies translate into psychiatry. *Mol. Psychiatry* https://doi.org/10.1038/s41380-020-0802-9 (2020).

Methods

Animals. Female Wistar rats aged 4–8 weeks were purchased from Janvier and housed under standard laboratory conditions (12-h light:dark cycle, lights on at 07:00, 22–24 °C, 50 ± 5% humidity, free access to food and water). All experiments were conducted under license G-102/17 (authorized by the German Animal Ethics Committee of the Baden Württemberg, Regierungspräsidium Karlsruhe) and in accordance with German law, under license 3668-2016011815445431 from the French Ministry and EU regulations. In total, 194 rats were used, of which 15 were excluded due to mistargeting or insufficient expression of viral vectors (Supplementary Table 3).

Viruses. The rAAVs (serotype 1/2) used in the present study (carrying the conserved region of the OT promoter and genes of interest in direct or 'floxed' orientations) were cloned and produced as reported previously[5,13,30,49]. HEK293T cells (Addgene, catalog no. 240073) were used for the virus production. The rAAVs produced included: rAAV-OTp-mCherry/Venus, rAAV-OTp-ChR2-mCherry, rAAV-OTp-DIO-ChR2-mCherry, rAAV-OTp-DIO-hM3D(Gq)-mCherry, rAAV-OTp-DIO-hM4D(Gi)-mCherry, rAAV-OTp-DIO-GFP, rAAV-OTp-DIO-ChR2-EYFP, rAAV-OTp-GCaMP6s, rAAV-OTp-TCB (TVA fused mCherry) and rAAV-Ef1A-DIO-oG. The CAV2-CMV-Cre was purchased from the Institute of Molecular Genetics[24]. The rAAVretro-Ef1A-Cre was purchased from the Salk Institute Viral Vector Core. Modified rabies virus was produced at the Gene Center Rabies laboratory, Ludwig Maximilian University.

Stereotactic injections of viral vectors. For stereotactic injections of viruses, rats were anesthetized with a mixture of ketamine (65 mg per kg birth weight) and xylazine (14 mg per kg birth weight). The rAAV genomic titers were determined using QuickTiter AAV Quantitation Kit (Cell Biolabs, Inc.) and reverse transcription PCR using the ABI 7700 cycler (Applied Biosystems). The rAAV titers were between 10^9 and 10^{10} genomic copies μl^{-1}. We injected 300 nl per PVN. CAV2-Cre was purchased from the Institute of Molecular Genetics (diluted to 10^9 genomic copies μl^{-1}, 300 nl per SON). Viruses were injected via a glass pipette into the target regions at 150 nl min^{-1} using a syringe pump as previously described[50]. Coordinates were chosen in accordance with a rat brain atlas[51] for PVN (anteroposterior (A/P): −1.8 mm; mediolateral (M/L): ±0.3 mm; dorsoventral (D/V): −8 mm), SON (A/P: −1.8 mm, M/L: ±1.2 mm, D/V: −9.25 mm) and posterior pituitary (A/P: −5.6 mm, M/L: ±0.1 mm, D/V: −10.5 mm). Verification of injection and implantation sites and expression of genes of interest was confirmed in all rats post hoc in 50-µm sections containing the PVN and SON (Histology).

Ex vivo experiments. *Slice preparation.* Some 4–8 weeks after injection of the viruses into the PVN and SON of 5-week-old virgin female rats, animals were anesthetized using ketamine (Imalgene 90 mg kg^{-1}) and xylazine (Rompun, 10 mg kg^{-1}) administered intraperitoneally. Then, intracardiac perfusion was performed with an ice-cold, *N*-methyl-D-glucamine (NMDG)-based artificial cerebrospinal fluid (aCSF), which contained (in mM): NMDG (93), KCl (2.5), NaH_2PO_4 (1.25), $NaHCO_3$ (30), $MgSO_4$ (10), $CaCl_2$ (0.5), 4-(2-hydroxyethyl)-1-piperazine-ethanesulfonic acid (Hepes) (20), D-glucose (25), L-ascorbic acid (5), thiourea (2), sodium pyruvate (3), *N*-acetyl-L-cysteine (10) and kynurenic acid (2). The pH was adjusted to 7.4 using either NaOH or HCl, after bubbling in 95% O_2/5% CO_2 gas. Rats were then decapitated, the brains removed and 350-µm-thick coronal slices containing the hypothalamus were obtained using a Leica VT1000s vibratome. Slices were warmed for 10 min in 35 °C NMDG aCSF and placed for a minimum of 1 h in a holding chamber at room temperature, containing normal aCSF. Normal aCSF, also used during all ex vivo experiments, is composed of (in mM): NaCl (124), KCl (2.5), NaH_2PO_4 (1.25), $NaHCO_3$ (26), $MgSO_4$ (2), $CaCl_2$ (2) and D-glucose (15), adjusted to a pH value of 7.4 with HCl or NaOH, and continuously bubbled with 95% O_2/5% CO_2 gas. All aCSF was checked for osmolality and kept to a value of between 305 and 310 mosmol. In electrophysiology or calcium-imaging experiments, slices were transferred from the holding chamber to an immersion recording chamber and superfused at a rate of 2 ml min^{-1}. CNO-containing solution (10 µM) was applied in a bath through a 6-min-long pumping episode, corresponding to several times the volume of the recording chamber (two applications per slice maximum). All ex vivo experiments were conducted at room temperature.

Patch-clamp recording. Whole-cell patch-clamp recordings were visually guided by infrared oblique light videomicroscopy (DM-LFS; Leica), using 4- to 9-MΩ borosilicate pipettes filled with a $KMeSO_4$-based intrapipette solution composed of (in mM): $KMeSO_4$ (135), NaCl (8), Hepes (10), $ATPNa_2$ (2) and GTPNa (0.3). The pH was adjusted to 7.3 with KOH and osmolality checked to be 300 mosmol l^{-1}, and adjusted with sucrose if needed. Data were acquired with an Axopatch 200B (Axon Instruments) amplifier and digitized with a Digidata 1440A (Molecular Devices). Series capacitances and resistances were compensated electronically. Data were sampled at 20 kHz and low-pass filtered at 5 kHz using the pClamp10 software (Axon Instruments). Further analysis was performed using Clampfit 10.7 (Molecular Devices) and Mini analysis v.6 software (Synaptosoft) in a semi-automated fashion (automatic detection of events with chosen parameters followed by a visual validation).

Evoked activity. To test the effects of CNO on neuronal excitability ex vivo, we used a current step method. For this purpose, we make PVN → SON projecting neurons express the DREADD receptors by injecting rats' SON with a CAV2-Cre virus (rAAV-CAV-Cre) and PVN with an OT-specific Cre-inducible DREADD construct (rAAV-OTp-DIO-hM4D(Gi)-mCherry or OTp-DIO-hM3D(Gq)-mCherry). Then, 6–8 weeks after infection, coronal slices were prepared and fluorescent neurons (indicative of the viral expression) were selected for whole-cell patch-clamp recordings. After establishing the clamp, neurons were recorded in current clamp mode with 0 pA injected. To test the effects of DREADD activation—hM4D(Gi) or hM3D(Gq)—neurons were subjected to the following current steps: for hM4D(Gi), neurons received an injection of an −100 pA negative current to hyperpolarize the neuron membrane (reaching −100 mV) before each step. These steps start at −80 pA and increase by 20 pA, reaching +120 pA. For hM3D(Gq), steps start at −20 pA and increase by 10 pA, reaching 80 pA. To quantify the effects of DREADD activation, the number of APs triggered by these steps was evaluated.

Spontaneous activity. To evaluate the effect of DREADD activation on neuronal activity, neurons were also recorded 2 min before and after CNO exposure in voltage or current clamp mode. In these cases, the frequency of the PSCs or APs was quantified.

Identification of parvOT and magnOT. The identity of PVN OT neurons was verified through a current step protocol[52]; this method has been used in several other studies to allow discrimination between parvocellular and magnocellular neurons[13,53–56]. Neurons received an injection of an −100 pA current to hyperpolarize the neuron membrane (reaching −100 mV) before each step. These steps start at 0 pA and increase by 20 A, reaching +60 pA. To discriminate between parvOT and magnOT, we have measured the hyperpolarizing notch and the T-outward rectification.

ChR2 stimulation of SON's parvOT neurons. To decipher the connection between SON parvOT neurons and PVN magnOT neurons, we used an optogenetic strategy. First, we identified PVN OT neurons by injecting rats' PVN with an rAAV containing the coding sequence of the fluorescent marker Venus, under the control of the OT promoter (OTp-Venus). Then, we aimed to specifically activate SON → PVN projection by using a combination of two rAAVs: the first was injected in the SON and induces the expression of the Cre recombinase in SON-targeting neurons, and the second was injected into the PVN to allow the expression of the ChR2 in OT neurons after a Cre-dependent recombination (OTp-DIO-ChR2-mCherry). Then, 6–8 weeks after infection, coronal slices containing the PVN were prepared and the $Venus^+$/$mCherry^-$ neurons were selected for whole-cell patch-clamp recordings. This combination of fluorescent markers allows us to select PVN OT neurons that are not directly targeting the SON.

Neurons were recorded for 2 min in the voltage clamp to establish the baseline frequency of PSCs and, then, we performed an optogenetic stimulation of ChR2-expressing oxytocinergic neurons by applying light pulses (10 ms at 30 Hz for 20 s) using light source X-Cite 110LED from Excelitas Technologies, through a GFP filter, controlled with a Clampex-driven TTL. Neurons were also recorded during the ChR2 stimulation to observe that the neurons were not expressing ChR2 itself. Finally, we continued to recorded 10 min after the stimulation to observe the effect of the SON parvOT neuron stimulation on the PSC frequency of the recorded neurons. PSCs were detected using Mini analysis v.6 software (Synaptosoft).

Calcium imaging. To test whether the chemogenetic activation of PVN → SON projecting oxytocinergic neurons can modify the intra-PVN microcircuit activity, we used an ex vivo calcium-imaging approach. To this end, rats' SON were infected with CAV2-Cre and the PVN with a virus allowing the expression of hM3D(Gq) under the control of OT promoter after a Cre-dependent recombination (OTp-DIO-hM3D(Gq)-mCherry). We also made PVN OT neurons express the calcium indicator GCaMP6s using a third viral vector (rAAV-OTp-GCaMP6s). Then, 6–8 weeks after infection, coronal slices containing the PVN were prepared and neurons that were positive for GCaMP, but negative for mCherry, were recorded. To perform this fluorescence microscopy, we used a Zeiss Axio examiner microscope with a ×40 water immersion objective (numerical aperture of 1.0), mounted with an X-Light Confocal unit—CRESTOPT spinning disk. Images were acquired at 5 Hz with an optiMOS sCMOS camera (Qimaging). Neurons within a confocal plane were illuminated for 100 ms at wavelength $\lambda = 475$ nm using a Spectra 7 LUMENCOR. The different hardware elements were synchronized through the MetaFluor software (Molecular Devices, LLC). Neuron calcium levels were measured in a hand-drawn region of interest (ROI). In all recordings, the Fiji rolling ball algorithm was used to increase the signal:noise ratio. Recordings in which movements/drifts were visible were discarded.

Offline data analysis was performed using a customized python-based script.

First, a linear regression and a median filter were applied to each trace. Peaks were then detected using the 'find_peaks' function of the SciPy library.

More precisely, fluorescence variation was identified as a calcium peak if its prominence exceeded twice the s.d. and if the maximum peak value surpasses three fluorescence units. The ROIs with zero calcium variations were excluded from the analysis. The remaining ROIs were considered as living neurons and the number of peaks quantified before and after the drug application. The AUC was estimated as the sum of the local area of each peak to avoid a biased AUC estimation due to baseline drift. All these data were normalized according to the duration of the recording and neurons were labeled as 'responsive' when their AUC or number of peaks was increased by at least 20% after drug application. As the time post-stimulation is longer than the baseline, the probability of observing a spontaneous calcium peak is stronger post-stimulation. To avoid this bias, neurons with only one calcium peak during the whole recording were removed from responsive neurons. The response probability was calculated as the number of responsive neurons with a least 1 calcium event per time bin (30 s) divided by the number of responsive neurons in each recording. Finally, all data were normalized per slice and this result was used as the statistical unit. All data were compared using paired statistical analysis (before versus after drug application) and the results are expressed as a ratio (baseline:drug effect), with a ratio of 1 meaning neither an increase nor a decrease in the measured parameter.

In vivo opto-electrode recordings. *Implantation of opto-electrodes.* Silicon probes (A1x32-Poly3-10mm, NeuroNexus) containing a 32-channel single shank combined with an optic fiber (diameter: 100 µm, Thorlabs) (opto-electrodes) were used in acute (anesthetized and head-fixed) recordings. For freely moving recordings, 32-channel chronic opto-electrodes were hand made, consisting of 8 tetrodes and 1 specially designed microdrive. The microdrives and tetrodes were manually assembled as described previously[57]. The tetrodes were made with 0.0005-inch tungsten wires (Stablohm 675, California Fine Wire Company). Eight tetrodes and an optic fiber (200 µm, Thorlabs) were loaded into the microdrive via a guiding tube and were arranged in parallel order. Assembled opto-electrodes were gold plated and the impedance of each channel was measured between 250 and 350 kΩ. For implantation, rats were anesthetized with 2% isoflurane and placed in a stereotaxic frame. Bregma position and horizontal level were aligned during the implantation. Opto-electrode tips were implanted into the target location and the microdrive was fixed on the skull by six microscrews (Knupfer) and dental cement (Paladur, Heraeus Kulzer).

Optogenetic identification of OT neurons. Electrophysiological signals were acquired by an Open-Ephys acquisition board and sampled at 30 kHz. To identify ChR2$^+$ OT neurons in the PVN, pulses of blue light (λ = 473 nm, DreamLasers) were delivered by the optic fiber while recording extracellular electrical activity of the neurons. The pulse train was controlled by a pulse generator (Master9, A.M.P.I.), and pulses had a duration of 10 ms and were applied at stimulation frequencies of 1, 5 and 10 Hz. In each session, the laser output at the optic fiber terminal was measured as 20 mW mm^{-2}. Neurons with a clear time-locked response to light pulses (spikes within 2–8 ms from onset of pulses) were classified as OT neurons (Extended Data Fig. 1e).

Analysis of spike waveforms. Spike sorting was done manually in Plexon Offline Sorter v.4.0 (Plexon, Inc.), with tetrode mode. The raw data were filtered at 250 Hz with a Butterworth high-pass filter, and waveform detection thresholds were placed at −0.5 to +0.8% of the analog-to-digital converter range (or −0.32 or ~−0.51 mV), depending on the signal:noise ratio. Magnocellular neurons have spikes with a width at half-amplitude of about 0.5 ms, an absolute refractory period of about 2.5 ms and a long relative refractory period, reflecting a prominent hyperpolarizing afterpotential[17]. Therefore, the sample length in waveform detection was set to 1.4 ms (400 µs pre-threshold period; at the 30-kHz sampling rate, a single waveform consists of 42 data points and, in the tetrode waveform, each unit detected 168 data points), and dead time was set to 1.2 ms. Next, the detected waveforms were aligned at the valley point, when the neurons were depolarized at their maximum, and principal component analysis and slice features of waveform were plotted and projected into 3D space for visual separation of clusters into presumptive single units. The timestamp feature was used to exclude mechanical noise recorded at the same time across four channels among the tetrodes. In different recording sessions (for example, OF and social interaction), we analyzed whether the features of spike waveforms remain consistent with the 3D plot results. After clustering, units with a minimum interevent interval exceeding 2,500 µs were accepted as single hypothalamic neurons. Units displaying minimum interevent intervals between 1,200 and 2,500 µs were recognized as arising from multiple neurons and excluded from the statistics of the study.

Statistical analyses of spike patterning. From segments of stationary activity recorded in OF conditions, interspike interval distributions were constructed to verify that these were consistent with distributions characteristic of OT neurons under basal conditions recorded in anesthetized rats[58]. To quantify the regularity of spike firing, we calculated the index of dispersion (IoD) of firing rate in 1-s bins as the ratio of the variance to the mean. For events that arise as a result of a random process that is invariant in time, the IoD will be equal to 1, independent of the mean rate and the binwidth. If events arise more regularly than chance, the IoD will be <1, and if they are more variable than expected by chance—as when spikes occur in clusters or bursts—the IoD will be >1.

In OT neurons, spikes cannot arise purely randomly because of the refractory period, and the IoD reduces slightly with increasing firing rate because, at higher rates, the relative refractory period is larger as a proportion of the mean interspike interval. The IoD also reduces with increasing binwidth because OT neurons also display a prolonged activity-dependent afterhyperpolarization that acts to stabilize mean firing rates over a timescale of seconds. Collectively the known intrinsic membrane properties of rat OT neurons, as tested through computational models, imply that, if spikes arise as a result of a purely random and time-invariant process, then the IoD of the firing rate in 1-s bins will be in the range 0.3–1.0 for neurons firing at up to 6 spikes s^{-1}, depending on firing rate and individual variability in membrane properties[17,58].

LFPs in the PVN. Local field potentials (LFPs) were sampled at 1 kHz with a low-pass filter. Subsequent analysis was done using customized MATLAB (MathWorks) scripts. We estimated the power spectrum density of the LFP signal using a multi-tapper approach, based on Thomson's method ('pmtm' function). Spectrograms were computed for each recording using a standard 'spectrogram' function. The power of theta oscillations was calculated as an average of power spectrum densities in the range 5–10 Hz. Phase-lock analysis was performed to investigate the relationship between theta oscillations in the PVN and the timing of spikes in OT neurons. The phase of the oscillatory activity was extracted with Hilbert's transformation ('Hilbert's' function) and converted into angle degrees. Then, we used Rayleigh's tests for circular uniformity, which indicate whether there is a significant correlation between the timing of spikes and a specific phase of the theta cycle (Extended Data Fig. 1h–j).

In vivo fiber photometry. *Optic-guided implantation of optic fibers.* We injected a modified adenovirus (AAV-OTp-GCaMP6s) bilaterally into the PVN or SON to transduce expression of the Ca^{2+} indicator GCaMP6s in OT neurons, and verified that this was expressed cell specifically (87 ± 4% of OT neurons, $n = 1{,}371$ neurons, $n = 4$ rats, Fig. 4p). Optic fibers (M127L01 diameter 400 µm, numerical aperture 0.50, length 10 mm, Thorlabs) were implanted ~100 µm above the dorsal border of the PVN (A/P: −1.8 mm; M/L: 0.35 mm; D/V: −7.85 mm) or SON (A/P: −1.25 mm; M/L: 1.90 mm; D/V: −9.0 mm) under 1.5% isoflurane anesthesia. Four 1-mm screws (Knupfer) and a metal implant guide (OGL, Thorlabs) were attached to the skull with OptiBond FL (Kerr) and fixed using dental cement (Paladur, Heraeus Kulzer).

During implantation, the implantable cannula was fixed in an adaptor (ADAL3, Thorlabs) attached to a stereotactic holder, whereas the other end of the cannula was connected through a pre-bleached Patch cord (Thorlabs, FP400URT) to the photodetector and light-emitting diode (LED) of the fiber photometry system (FOM, NPI Electronic). The digitized photometry signal was monitored and recorded via a digital input/output board (Open-Ephys) to the DAQ system (Open Ephys) with 0.1- to 20-Hz bandpass filter and 20-s timescale set in to visualize the Ca^{2+} signal online, while the cannula tip was gradually lowered into the PVN at 1 mm min^{-1}. When the optic fiber tip was close to the PVN where GCaMP6s was expressed, a slight increase in the signal baseline and a minor spontaneous fluctuation could be visually detected. During implantation, rats were under 1.5% isoflurane anesthesia and the body temperature was kept stable at 37 °C by a heating plate (Temperature controller 69001, RWD Life Science). The LED power in the fiber photometry system was set at a constant value between 5 and 10 mW mm^{-2}. The fiber photometry recordings were conducted after 1 week of recovery from the implantation. Fiber photometry raw data were sampled at 30 kHz in Open-Ephys GUI and analyzed with customized MATLAB scripts.

Fiber photometry data analysis. Digitized optical signal acquired from the fiber photometry system was first downsampled at 3,000 Hz and then low-pass filtered (MATLAB 'butterworth' function) at 10 Hz to exclude noise at higher frequency. Second, to correct the baseline drifting due to photo-bleaching of fluorophores, we fitted the signal with a polynomial curve (MATLAB 'polyfit' function) and subtracted it from the signal. Next, we smoothed the signal with a Savitzky–Golay filter (MATLAB 'smooth' function, option 'sgolay'). For each experiment, the signal F was converted to $\Delta F/F_0$ by:

$$\Delta F/F(t) = \frac{F(t) - F_0}{F_0}$$

where t is time and F_0 was calculated as the average value of F of a 600-s recording at the start of the experiment. The data were subdivided into 1-min bins and the mean $\Delta F/F_0$ was calculated for each bin. We detected calcium transients similar to those reported in our previous study[59]. Finally, we calculated the AUC of the Ca^{2+} signal (MATLAB 'trapz' function) to estimate the cumulative fluorescence for each bin and normalized the AUC to values from 0 to 1. Values of normalized AUC were displayed in a 1-min bin and averaged in 30-min bins. The ratios of AUCs between experimental and control conditions were used for quantitative analysis and called 'relative AUC increase'.

Application of airpuffs and OT neuron response. Airpuffs from a pressurized air can (Toolcraft, 20793T, 400 ml) were applied through a stiff micropipette tip with a 2-mm opening positioned 10–15 mm above the skin in an area of ~2 cm^2. A plastic cover with 2-cm holes was placed above the rat's body to restrict the area of stimulation. The controlled air pressure was 1.139 g cm^{-3}. During in vivo electrophysiology recordings, in each stimulation point, five airpuffs (duration 0.2 s, interval between puffs 1 s) were delivered in sequence with intervals of 1 min between sequences (Fig. 2a and Extended Data Fig. 4). During fiber photometry recordings, one airpuff (duration 1 s) was applied every 1 min (Fig. 2e–j).

OT neuron response to airpuff stimulations. We applied airpuffs to the skin of three regions of the rat's dorsal body area (anterior, central and posterior parts), two regions of the rat's ventral area (abdomen and anogenital area) and the whiskers on both sides. We considered a recorded neuron as responsive to airpuff stimulations if the average firing rate after (from 0 s to 2 s) stimulus onset increased by at least twice the s.d. of the baseline activity (2 s before stimulus onset). Onset of the response was calculated as the time at which the firing rate of a responsive neuron increased by 1× the s.d. of the baseline activity. We recorded the activity of $n = 23$ OT neurons in response to airpuffs applied to the rat's dorsal body area, which showed variable response latencies of up to 30 s (Extended Data Fig. 4a,b); 10 of those neurons exhibited a response within 1 s after stimulus onset and are shown in Fig. 2a,b.

Blood sampling and plasma OT measurements. To monitor neurohypophyseal OT release after chemogenetic activation of hypothalamic parvOT neurons, we performed blood sampling from the jugular vein in urethane-anesthetized rats. After surgery, rats were placed on a heating pad for the rest of the experiment to maintain constant body temperature. The jugular vein catheter was connected to a 1-ml syringe containing sterile heparinized saline (30 U ml^{-1}); 45 min before, and 45 min as well as 90 min after, intraperitoneal CNO, 500 µl blood was drawn (Fig. 4q,r), which was replaced by 500 µl sterile saline. After each sample, the catheter was filled with heparinized saline to avoid blood clotting. Blood samples were collected in ethylenediaminetetraacetic acid (EDTA) tubes (Bayer) on ice, centrifuged (5,000*g*, for 10 min at 4 °C), and 200-µl plasma samples were stored at −80 °C before extraction and OT quantification by radioimmunoassay. The OT content in extracted plasma was analyzed by a highly sensitive radioimmunoassay with a detection limit of 0.1 pg and cross-reactivity <0.7% (RIAgnosis)[60,61].

Behavior. Starting from 14 d before behavioral tests, vaginal smears were collected to monitor ovarian cycle. Rats in the metestrus, proestrus and estrus phases were excluded from the experiments and reintroduced once they reached diestrus.

Behavioral tests were conducted in an arena (material nonabsorbent to odors) with dimensions 60 × 60 × 60 cm^3 under dim light conditions (<20 lux; lux-meter SO 200K, Sauter). On the day before the test, the experimental rat was exposed to the arena for 15 min for habituation. The arena was cleaned with 70% ethanol after each session to eliminate residual odors. Experimental and stimulus rats were housed in separate cages and had not previous encountered each other before the social interaction tests. The same rat was exposed to social interaction tests twice on separate days, each time with a different social stimulus rat so that the experimental paradigm always represented interaction with a novel, unfamiliar conspecific.

OF test. The experimental rat was placed in a corner of the arena and was allowed to freely explore the environment. These tests served as a 'baseline' for social interaction tests.

FSI test. The experimental and the stimulus rats were placed in opposite corners of the arena at the same time and were allowed to freely interact with each other and/or explore the environment.

CSI test. For this test, two Plexiglas transparent meshes (dimensions 20 × 30 × 1 cm^3) provided with three openings/holes (dimensions 15 × 0.75 cm^2) were placed in two opposite corners of the arena. The mesh separated a little triangular area (14 × 14 × 20 cm^3, corresponding to ~3% of the total area of the arena) from the rest of the arena (central compartment). The experimental rat was placed in the central compartment whereas the stimulus rat was placed in one of the two little compartments. The two rats were able to see, hear and smell each other through the openings, but they were not able to touch each other.

Chemogenetic inhibition or activation of parvocellular OT neurons by DREADD. To selectively activate or inhibit parvocellular OT neurons, rats were injected with rAAV-OTp-DIO-hM3D(Gq)-mCherry (Parvo-Gq group), rAAV-OTp-DIO-hM4D(Gi)-mCherry (Parvo-Gi group) or rAAV-OTp-DIO-GFP (Parvo-GFP control group) into the PVN and CAV2-Cre into the SON, as previously described[13].

All groups (Parvo-Gq, Parvo-Gi and Parvo-GFP) were subjected to the same protocol. On day 1 experimental rats were exposed to the OF arena for 15 min for habituation. On day 2, the experimental rat was injected intraperitoneally with either CNO or saline solution 60 min before starting the tests, and was then subjected to one CSI and one FSI session for 5 min each.

Intracerebroventricular administration of OTR antagonist. Guide cannulas were implanted above the lateral ventricle for intracerebroventricular infusion of the OTR antagonist *des*-Gly-NH_2,*d*$(CH_2)_5$(Tyr(Me)^2,Thr^4)OVT[29]. OTR antagonist 0.75 µg per 5 µl (ref. [30,62]) was infused 15 min before the behavioral tests. Four groups of rats were studied, which received intraperitoneal injection and intracerebroventricular infusion of saline/saline, CNO/saline, saline/OTR antagonist or CNO/OTR antagonist, respectively.

Video and audio analyses of behavior. The videos were recorded using a GigE color HD camera (Basler AG). The tracks of the experimental and stimulus rats were extracted from videos using two software packages: Ethovision XT v.11.5 (Noldus) and MATLAB Toolbox idTracker (MathWorks). The results of the two software packages were compared and crossvalidated. The distance moved by each rat, the velocity, time spent in different areas of the arena, and distance between rats and time spent in close proximity were calculated automatically. Social interactions were also analyzed manually to classify social behaviors into different categories: 'sniffing', 'chasing', 'crawling on top', 'being crawled' and 'head-to-head' approaching; the time spent by the experimental rat for each behavioral category was used for all analyses. Manual scoring of social behavior scoring was done by a researcher (different from the person who performed the experiment) who was blind to treatment conditions.

Ultrasonic vocalizations were recorded with an ultrasound microphone (Avisoft-Bioacustic) and analyzed using Avisoft-SASlab Pro v.5.2 software. After calculation of a sound spectrogram, the vocalization time, duration and frequency were extracted. Each 'call' was classified into a non-social (peak frequency ~22 kHz) or an appetitive/social (peak frequency ~50 kHz) call. Social vocalizations were further classified into trills (<10 ms), single component calls (>10 ms, not modulated) and complex vocalizations (>10 ms, frequency modulated or combined)[63].

Freely moving single unit recordings: experimental groups. Open field and FSI groups: experimental rats implanted with opto-electrodes for single-unit recordings in the PVN were subjected to one OF session and one FSI session for 10 min each. Between the two sessions the rat was placed in the home cage (single housed) for 15 min.

Open field, CSI and FSI groups: experimental rats implanted with opto-electrodes for single-unit recordings in the PVN were subjected to one OF, one CSI and one FSI session for 10 min each, without pauses in between. Stimulus rats were placed in one of the little chambers separated by a Plexiglas mesh at the start of the CSI session; the wall was then lifted up (Fig. 6b) at the start of the FSI session, allowing the stimulus rat to join the experimental rat in the central compartment.

Histology. Anesthetized rats were transcardially perfused with phosphate-buffered saline (PBS) followed by 4% paraformaldehyde (PFA). Brains were dissected out and post-fixed overnight in 4% PFA at 4 °C with gentle agitation. Then, 50-µm vibratome coronal sections containing the PVN and the SON were cut and collected. Immunohistochemistry was performed on free-floating sections using the following antibodies: anti-OT (PS38, 1:2,000; mouse; kindly provided by H. Gainer), anti-OT (T-5021, 1:50,000, Peninsula, guinea-pig), anti-SYN (Abcam, anti-rabbit, ab32127, 1:1,000), anti-Ds-Red (Clontech, catalog no. 632397, 1:1,000; rabbit), anti-GFP (Abcam, ab13970, 1:1,000, chicken), anti-*c-fos* (Cell Signaling, catalog no. 9F6, 1:500, rabbit), anti-Fluorogold (Protos Biotech. catalog no. NM-101, 1:1,000, guinea-pig) and anti-Cre (Novagen, catalog no. 69050, 1:2,000, mouse). Further information on validation of primary antibodies can be found in the Nature Research Reporting Summary. The signals were visualized with the following secondary antibodies: CysTyr3 conjugate (711-165-152) or CysTyr5 conjugate (Jackson Immuno-Research Laboratories, 115-175-146) or Alexa 488 (Invitrogen, A11039) and Alexa 594 (Invitrogen, A11012) and Alexa-594 (Jackson Immuno-Research Laboratories, 715-585-151) and Alexa-647 (Jackson Immuno-Research Laboratories, 713-645-147). All secondary antibodies were diluted 1:500.

Fluorogold treatment and visualization. To discriminate between magnOT and parvOT neurons, rats received a single injection of Fluorogold (Santa Cruz Biotechnology, 15 mg per kg birth weight intraperitoneally) 7 d before the perfusion. Brain sections were stained with a primary antibody for Fluorogold (guinea-pig anti-FG, dilution 1:1,000, Protos Biotech Corp) and Fluorogold immunosignal was visualized by secondary antibodies conjugated with CysTyr3 (Jackson Immuno-Research Laboratories, goat anti-rabbit, dilution 1:500). The co-localization of Fluorogold, OT and *c-fos* signals was manually quantified in the PVN ($n = 4$ rats, 6 sections per brain).

Images of immunostained tissue sections. All images were acquired on a Leica TCS SP5 (DKFZ Light Microscopy Facility), confocal laser-scanning microscope. Digitized images were analyzed using Fiji (National Institute of Mental Health) and Adobe Photoshop CS5 (Adobe).

Confocal microscopy and 3D IMARIS analysis. For the 3D reconstruction of OT neurons, we took *z*-stack images (50 µm depth, 1-µm steps, ×40 magnification) of PVN and SON using a Zeiss LSM 780 confocal microscope (1,024 × 1,024 pixels, 16-bit depth, pixel size 0.63 µm, zoom 0.7). Raw czi files were used for further analysis with IMARIS[26,27,64] software (v.9.31, Oxford Instruments: https://imaris.oxinst.com). First, IMARIS was used to reconstruct the cellular surface using the following customized settings: surface detail 0.700 µm (smooth); thresholding background subtraction (local contrast), diameter of largest sphere, which fits into the object: 2.00; color: base; diffusion transparency: 65%. After surface reconstruction, we used the filter function to remove unspecific background signals: filter: volume maximum 400 µm^3. After deletion of all background signals the 'mask all' function was used to create the final surface reconstruction. Next, the surface reconstruction was used as the template for the filament reconstruction using the following customized settings: detect new starting points: largest diameter 7.00 µm, seed points 0.300 µm; remove seed points around starting points: diameter of sphere regions: 15 µm. Seed points were corrected for (either placed in or removed from the center of the somata) manually if the IMARIS algorithm placed them incorrectly. All surface and filament parameters were exported into separate Excel files and used for data analysis. For all quantifications, we used 6–8 ×40 *z*-stacks per animal (2 *z*-stacks per brain hemisphere). We used a computer suited for IMARIS analysis (Intel Core i7 8700 @ 3.2 GHz, 64 GB RAM, x-64-bit, Windows 10 Enterprise). All images used for analysis were taken with the same confocal settings (pinhole, laser intensity, digital gain and digital offset). Sholl analysis was performed using IMARIS in the filament reconstruction mode and individual datasets were exported into separate Excel files for further analysis. To assess the number of SYN$^+$/GFP$^+$ axons, we used a simplified version of the Sholl analysis, where we included only the first two to eight spheres (starting in the soma center) until either we could detect SYN$^+$/GFP intersections or they were >2 µm apart from the border of the respective soma. The total amount of immunofluorescence (SYN) was calculated using the extract intensity/number of spots function. First, we created spheres that precisely engulfed the respective somata (parvOT and magnOT neurons) so that both ends of the cell soma (maximum diameter) touched the border of the respective sphere. To account for individual variability in roundness and surface area, we calculated the surface area for each individual OT cell using the surface reconstruction mode. Given that cells with a larger surface area occupy more 3D space within the artificially constructed sphere, which could confound precise quantification of SYN fluorescence, we adjusted each calculated value (SYN$^+$ voxels per sphere) based on the surface area. Assuming an inverse almost-linear relationship between cell volume and the total amount of SYN fluorescence within a sphere, we calculated the degree of occupancy (that is, percentage) for each soma within the respective sphere. Finally, we calculated the final SYN$^+$ voxels using the following equation: (Number of SYN$^+$ voxels) × (Degree of occupancy). For the quantification along the dendrites we used spheres with a 10-µm radius along the dendrite for both parvOT and magnOT neurons.

Projection-specific, trans-synaptic retrograde tracing. Input tracing experiments were performed in female Wistar rats (aged 10–12 weeks). We used Rb-GFP[28] to monosynaptically retrogradely trace neurons projecting to parvOT and magnOT neurons. Rb-GFP selectively enters neurons expressing the avian sarcoma and leukosis virus receptor (TVA), and can spread presynaptically only from neurons expressing the rabies virus glycoprotein (we used the optimized glycoprotein, oG, used previously[65]). We injected a 300 nl mixture of 1:1 rAAV-OTp-TCB:rAAV-Ef1A-DIO-oG into the right PVN of female rats. Then, to specifically trace inputs to parvOT neurons, we injected rats ($n = 5$) with CAV2-CMV-Cre into the right SON (Extended Data Fig. 8a). In another group of rats ($n = 5$), we employed a similar strategy to express oG only in magnOT neurons: we injected an AAV retrograde-expressing Cre (rAAVretro-Ef1A-Cre) into the posterior pituitary (Extended Data Fig. 8c, based on previous work[66]). This strategy makes Rb-GFP selectively enter all OT neurons, but specifically spread retrogradely from neurons expressing oG (that is, parvOT or magnOT neurons). After 2 weeks, we injected 300 nl EnvA ΔG-EGFP into the right PVN, and, 7 d later, animals were perfused with 4% PFA. The number of projecting neurons was quantified from brain sections as follows: every third 50-µm section was imaged and neurons were counted, and then multiplied by three, to estimate the real number of inputs. GFP$^+$ neurons on the injected hemisphere were counted and assigned to brain areas based on classifications of the Paxinos Mouse Brain Atlas[37], using anatomical landmarks in the sections visualized by tissue autofluorescence. Very few contralateral inputs were noticed and we therefore decided to neglect them. Although we had good infection at injection sites for both parvOT and magnOT groups (Extended Data Fig. 8g), starter neurons could not be reliably counted, because rabies virus toxicity prevented us correctly visualizing mCherry in the PVN. Thus, the analysis presented here does not take into account inputs to OT neurons from within the PVN. The percentage of inputs from each region was obtained by dividing the number of inputs from one region by the total number of inputs. Input regions that were detected in a subset of animals only were discarded from the analysis. We used unpaired, two-sided Student's *t*-tests to compare the total number of inputs with parvOT and magnOT neurons and χ^2 tests to compare proportions of inputs between regions.

We controlled TVA being selectively expressed in OT neurons by injecting control rats ($n = 2$) with rAAV-OTp-TCB in the PVN, and staining for OT. This revealed that most OT neurons expressed mCherry and no non-OT neurons expressed mCherry (Extended Data Fig. 8e). Furthermore, we verified that Rb-GFP was selectively entering OT neurons by injecting control rats ($n = 2$) with rAAV-OTp-TCB, and Rb-GFP 2 weeks later. This resulted in specific expression of GFP in PVN OT neurons (Extended Data Fig. 8f).

In each rat, we confirmed the SON injection site by staining for Cre for the parvOT neurons tracing (Extended Data Fig. 8a,b) and injecting a virus Cre-dependently expressing mCherry in the SON of magnOT neuron tracing, which led to expression of mCherry in SON magnocellular neurons (Extended Data Fig. 8c,d).

OT secretion model. The OT secretion model[17] simulates stimulus-secretion coupling in OT neurons. The model is a continuous approximation of the stochastic release process from all neuronal compartments. It is based on extensive studies on activity-dependent hormone secretion from magnocellular neurosecretory neurons[58] and it matches experimental data closely. In the model, when spikes invade the secretory terminals, exocytosis occurs in response to fast rising Ca^{2+} concentrations (e). At higher frequencies, the spikes broaden, producing a larger increase in e. The rate of secretion is modeled as the product of: e raised to the power of φ (which accounts for the cooperativeness of the Ca^{2+} activation), of the pool of releasable OT p, and a secretion-scaling factor α, and is calculated as:

$$s = e^{\varphi} \times \alpha \times p$$

where $\varphi = 2$ and $\alpha = 0.003\ \mathrm{pg\,s^{-1}}$.

The nonlinear dependence of the secretion rate gives high secretion probability on short spike intervals. To infer OT secretion arising from the spike trains observed in the present study, the recorded event timings were used to drive the secretion model described fully elsewhere[17]. The published model is scaled to quantitatively match secretion from the pituitary nerve terminals of a single OT neuron. The scaling factor α cannot be used for absolute quantitative estimates of release within the brain, but the relative efficacy of two firing patterns can be compared using the model, because α is eliminated in the ratio.

Statistics. Statistical analyses were performed using SigmaPlot v.11 (Systat) and GraphPad Prism v.7.05 (GraphPad Software). The two-sided, Wilcoxon's signed-rank *W*-test was used to compare the variation of spike frequencies measured for the same neuron in different conditions. The two-sided Mann–Whitney *U*-test was used to compare low threshold depolarization in different cells. Two-sided Student's *t*-tests were used to compare average values in two conditions when the data satisfied assumptions of normality. Pearson's correlation coefficient was used to measure the linear correlation between firing rate and animals' distance. One-way analysis of variance (ANOVA), followed by a multiple comparison post hoc test, was used to compare averages in three or more conditions. Two-way ANOVA, followed by a multiple comparison post hoc test, was used to analyze electrophysiological or behavioral data with repeated measures and CNO/saline/OTR antagonist treatment (time × treatment). No statistical methods were used to predetermine sample size, but our sample sizes are similar to those reported in previous publications[5,13,30].

Differences were considered significant for $P < 0.05$. Asterisks were used to indicate the significance level: $^*0.01 \le P < 0.05$, $^{**}0.001 \le P < 0.01$, $^{***}P < 0.001$. Statistical analyses of neuronal spike trains and local field potentials, such as PSTHs, auto- and cross-correlation, spike burst analysis, power spectrum density and phase locking were performed using NeuroExplorer 3 (Nex Technologies) and customized MATLAB scripts.

Randomization and blinding. Randomization was used to assign brain samples and animals to experimental groups whenever possible, with the constraint that, in social behavior experiments, interacting rats had to be unfamiliar conspecifics, as described under Methods.

Most of the measurements were made using a machine, and are not subject to operator bias, with the exception of manual scoring of social behaviors from videos; in this case, all scorings were done by a researcher (different from the one who performed the experiment) who was blind to treatment conditions.

Reporting Summary. Further information on research design is available in the Nature Research Reporting Summary linked to this article.

Data and code availability

Python code (used for ex vivo calcium-imaging data analysis in Fig. 4a–d) and MATLAB code (used for in vivo fiber photometry data analysis in Fig. 4e–o and Extended Data Fig. 7a–n) can be found in Supplementary Software. All data that support the findings of the present study, as well as MATLAB codes for the analysis of extracellular recording data, are available from the corresponding author upon reasonable request.

References

49. Menon, R. et al. Oxytocin signaling in the lateral septum prevents social fear during lactation. *Curr. Biol.* **28**, 1066–1078.e6 (2018).
50. Grinevich, V. et al. Somatic transgenesis. *Viral Vectors* **3**, 243–274 (2016).
51. Paxinos, G. & Watson, C. *The Rat Brain in Stereotaxic Coordinates*, 7th edn (Elsevier Acad. Press, 2014).
52. Tasker, J. G. & Dudek, F. E. Electrophysiological properties of neurones in the region of the paraventricular nucleus in slices of rat hypothalamus. *J. Physiol.* **434**, 271–293 (1991).
53. Chu, C.-P. et al. Effects of stresscopin on rat hypothalamic paraventricular nucleus neurons in vitro. *PLoS ONE* **8**, e53863 (2013).
54. Luther, J. A. & Tasker, J. G. Voltage-gated currents distinguish parvocellular from magnocellular neurones in the rat hypothalamic paraventricular nucleus. *J. Physiol.* **523**, 193–209 (2000).
55. Luther, J. A. et al. Neurosecretory and non-neurosecretory parvocellular neurones of the hypothalamic paraventricular nucleus express distinct electrophysiological properties. *J. Neuroendocrinol.* **14**, 929–932 (2002).
56. Yuill, E. A., Hoyda, T. D., Ferri, C. C., Zhou, Q.-Y. & Ferguson, A. V. Prokineticin 2 depolarizes paraventricular nucleus magnocellular and parvocellular neurons. *Eur. J. Neurosci.* **25**, 425–434 (2007).
57. Tang, Y., Benusiglio, D., Grinevich, V. & Lin, L. Distinct types of feeding related neurons in mouse hypothalamus. *Front. Behav. Neurosci.* **10**, 91 (2016).
58. Maícas Royo, J., Brown, C. H., Leng, G. & MacGregor, D. J. Oxytocin neurones: intrinsic mechanisms governing the regularity of spiking activity. *J. Neuroendocrinol.* **28**, 28 (2016).
59. Grund, T. et al. Chemogenetic activation of oxytocin neurons: temporal dynamics, hormonal release, and behavioral consequences. *Psychoneuroendocrinology* **106**, 77–84 (2019).
60. de Jong, T. R. et al. Salivary oxytocin concentrations in response to running, sexual self-stimulation, breastfeeding and the TSST: the Regensburg Oxytocin Challenge (ROC) study. *Psychoneuroendocrinology* **62**, 381–388 (2015).
61. Landgraf, R., Neumann, I., Holsboer, F. & Pittman, Q. J. Interleukin-1β stimulates both central and peripheral release of vasopressin and oxytocin in the rat. *Eur. J. Neurosci.* **7**, 592–598 (1995).
62. Neumann, I. D., Maloumby, R., Beiderbeck, D. I., Lukas, M. & Landgraf, R. Increased brain and plasma oxytocin after nasal and peripheral administration in rats and mice. *Psychoneuroendocrinology* **38**, 1985–1993 (2013).
63. Ishiyama, S. & Brecht, M. Neural correlates of ticklishness in the rat somatosensory cortex. *Science* **354**, 757–760 (2016).
64. Althammer, F., Ferreira-Neto, H. C., Rubaharan, M., Roy, K. R. & Stern, J. E. Three-dimensional morphometric analysis reveals time-dependent structural changes in microglia and astrocytes in the central amygdala and hypothalamic paraventricular nucleus of heart failure rats. *Res. Sq.* https://doi.org/10.21203/rs.3.rs-22630/v1 (2020).
65. Kim, E. J., Jacobs, M. W., Ito-Cole, T. & Callaway, E. M. Improved monosynaptic neural circuit tracing using engineered rabies virus glycoproteins. *Cell Rep.* **15**, 692–699 (2016).
66. Zhang, B. et al. Reconstruction of the hypothalamo-neurohypophysial system and functional dissection of magnocellular oxytocin neurons in the brain. Preprint at *bioRxiv* https://doi.org/10.1101/2020.03.26.007070 (2020).

Acknowledgements

We thank T. Grund and X. Liu for initial contribution to this study, R. Stoop for valuable comments on the manuscript, J. Müller for packaging viral vectors, E. Kremer for the canine virus, J. Maicos-Roya for contributing to the modeling of OT release, S. Netser for his comments on the manuscript, C. Pitzer and the Interdisciplinary Neurobehavioral Core Facility of Heidelberg University for some of the behavioral experiments performed there, and T. Splettstoesser (www.scistyle.com) for composing Extended Data Fig. 10. The work was supported by Chinese Scholarship Council No. 201406140043 (to Y.T.), the German Research Foundation (DFG) within the Collaborative Research Center (SFB) 1158 seed grant for young researchers and Fyssen Foundation (to A.L.), DFG postdoctoral fellowship AL 2466/1-1 (to F.A.), Alexander von Humboldt research fellowship (to D.H.), Human Frontier Science Program RGP0019/2015 (to V.G. and S.W.), Israel Science Foundation (grant nos. 1350/12 and 1361/17), Milgrom Foundation and the Ministry of Science, Technology and Space of Israel (grant no. 3-12068, to S.W.), NIH grant (no. R01NS094640, to J.E.S.), BBSRC grant (no. BB/S000224/1, to G.L.), DFG grant (nos. NE 465/27, NE 465/31 and NE 465/34, to I.D.N.), ANR-DFG grant and PICS grant (no. GR 3619/701 and no. GR 07882, to A.C. and V.G.), NARSAD Young Investigator grant (no. 24821) and ANR JCJC grant (no. GR 19-CE16-0011-01, to A.C.), DFG grant (no. GR 3619/4-1), SFB 1158, SNSF-DFG grant (no. GR 3619/8-1) and Fritz Thyssen Foundation grant (no. 10.16.2.018 MN) (all to V.G.).

Author contributions

Y.T., D.B., A.L., A.C. and V.G. designed and conceived the project. L.H. and P.D. performed the ex vivo electrophysiology. L.H. and A. Baudon did the ex vivo calcium imaging. Y.T., D.B. and S.W. performed the in vivo electrophysiology. Y.T. and A.L. did the fiber photometry. Y.T., D.B. and S.W. performed the behavioral experiments and analyses. D.B., M.E., D.H. and F.A. did the immunohistochemistry and confocal microscopy. A.L. and J.S. performed the trans-synaptic labeling of OT neuron inputs. M.S., M.O. and K.K.C. assisted with virus design for trans-synaptic labeling. F.A., M.K.K., R.K.R. and J.E.S. did the 3D reconstruction and analysis. A. Bludau and I.D.N. calculated the plasma OT dosages. G.L. did the modeling. Y.T., D.B., A.L., L.H., F.A., I.D.N., A.C. and V.G. prepared the manuscript. I.D.N., A.C. and V.G. supervised and administered the project, and acquired the funding.

Competing interests

The authors declare no competing interests.

Additional information

Extended data is available for this paper at https://doi.org/10.1038/s41593-020-0674-y.

Supplementary information is available for this paper at https://doi.org/10.1038/s41593-020-0674-y.

Correspondence and requests for materials should be addressed to A.C. or V.G.

Peer review information *Nature Neuroscience* thanks Dayu Lin, Jeffrey Tasker and the other, anonymous, reviewer(s) for their contribution to the peer review of this work.

Reprints and permissions information is available at www.nature.com/reprints.

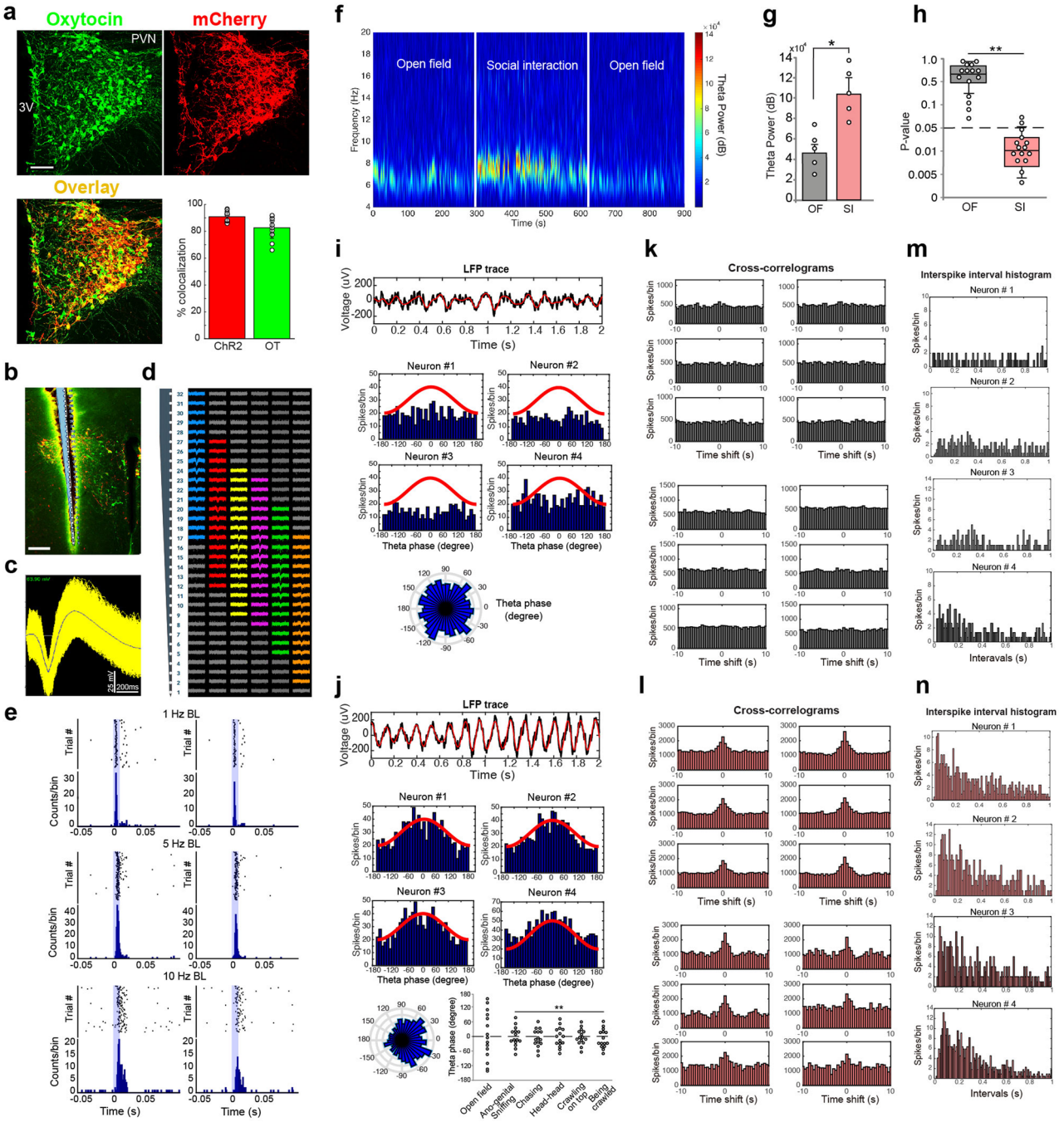

Extended Data Fig. 1 | See next page for caption.

Extended Data Fig. 1 | Recording of optogenetically identified oxytocin neurons, local field potential, phase locking, synchronization and spike distribution. a, The cell type specificity of rAAV-OTp-ChR2-mCherry expression in OT cells. OT-immunosignal (green) colocalizes with ChR2-mCherry (red) signal; the overlay appears in yellow. Scale bar = 100 μm. Bottom, right: quantification of the colocalization mCherry/ChR2 (red bar, 90.8 ± 3.9 %) and mCherry/OT immnoreactive cells (green bar, 82.6 ± 7.7 %). Bar plots show mean ± SEM. **b**, Post-hoc verification of implanted optoprobe location in the PVN in a representative animal (one of five rats). Scale bar = 100 μm. **c**, Sorted extracellular spike waveforms (n = 175 action potentials) of a representative single unit optically-identified as OT neurons. **d**, Silicon probe (NeuroNexus) with 32-channel single shank were used in acute (anesthetized) single units recording. Sorted units and their location in the channels map were visualized with Phy-GUI (klusta, Python). Spike sorting was manually done in Plexon Offline Sorter 4.0 (Plexon, Inc.). **e**, PSTHs illustrating two optogenetically-identified oxytocin neurons by their response to blue light pulses (1 Hz, 5 Hz and 10 Hz laser stimulation, 10 ms, λ=473 nm, 10 mW/mm^2). In both neurons, low frequency stimulation evoked spikes with a relatively constant short latency of 2-10 ms. **f**, Power spectrogram of the local field potential (LFP) in the PVN recorded before (open field, OF), during and after (OF) a free social interaction (FSI) session. **g**, Average theta (5-10 Hz) power recorded during and FSI session is significantly higher than before FSI session ($p = 0.03$, n = 5 rats, paired two-sided t test). All data represented as mean + SEM. **h**, P value distribution of phase-locking between theta (5-10 Hz) oscillations and OT cells spikes during exploratory (OF) or social (FSI) behavior (** $p = 0.0089$, n = 15 cells from 5 rats, paired two-sided t test; box plot shows median 10th, 25th, 75th, and 90th percentiles; min/max: OF, 0.07/0.99; SI, 0.002/0.08). **i, j**, Example traces (black) of LFP in the PVN and band-pass (5-10 Hz) filtered theta oscillations (red) during exploratory (OF) or social (FSI) behavior. Examples of distribution of four OT neurons firing in relation to LFP theta oscillations; OT neurons spikes are phase-locked with theta oscillations (** $P = 0.0014$, n = 15 cells) during social interaction (FSI, **j**), but not during exploratory behavior (**i**). Circular representation of OT neurons firing in relation to theta oscillation phase shows phase locking during social behavior (**l**) exclusively. No significant difference of spike-phase coupling between social behavior subtypes ($P = 0.28$). Significance of phase locking are determined by Rayleigh test for circular uniformity. **k, l**, Cross-correlation of pairs of oxytocin neurons recorded simultaneously. During open field (**k**) test there is no detectable correlation between oxytocin neurons spiking activity, but during social interaction (**l**) there is a significant increase ($P = 0.0038$, n = 12 cell pairs) of temporally correlated spikes within a time window of $\tau = 1.2 \pm 0.5$ s (mean correlation half-time). **m, n**, Examples of interspike interval (ISI, time bins = 10 ms) histograms of four OT neurons recorded during exploratory behavior (OF, **m**) and during social interaction (FSI, **n**). During FSI there is a prominent increase of spikes with short intervals due to increased spike clustering.

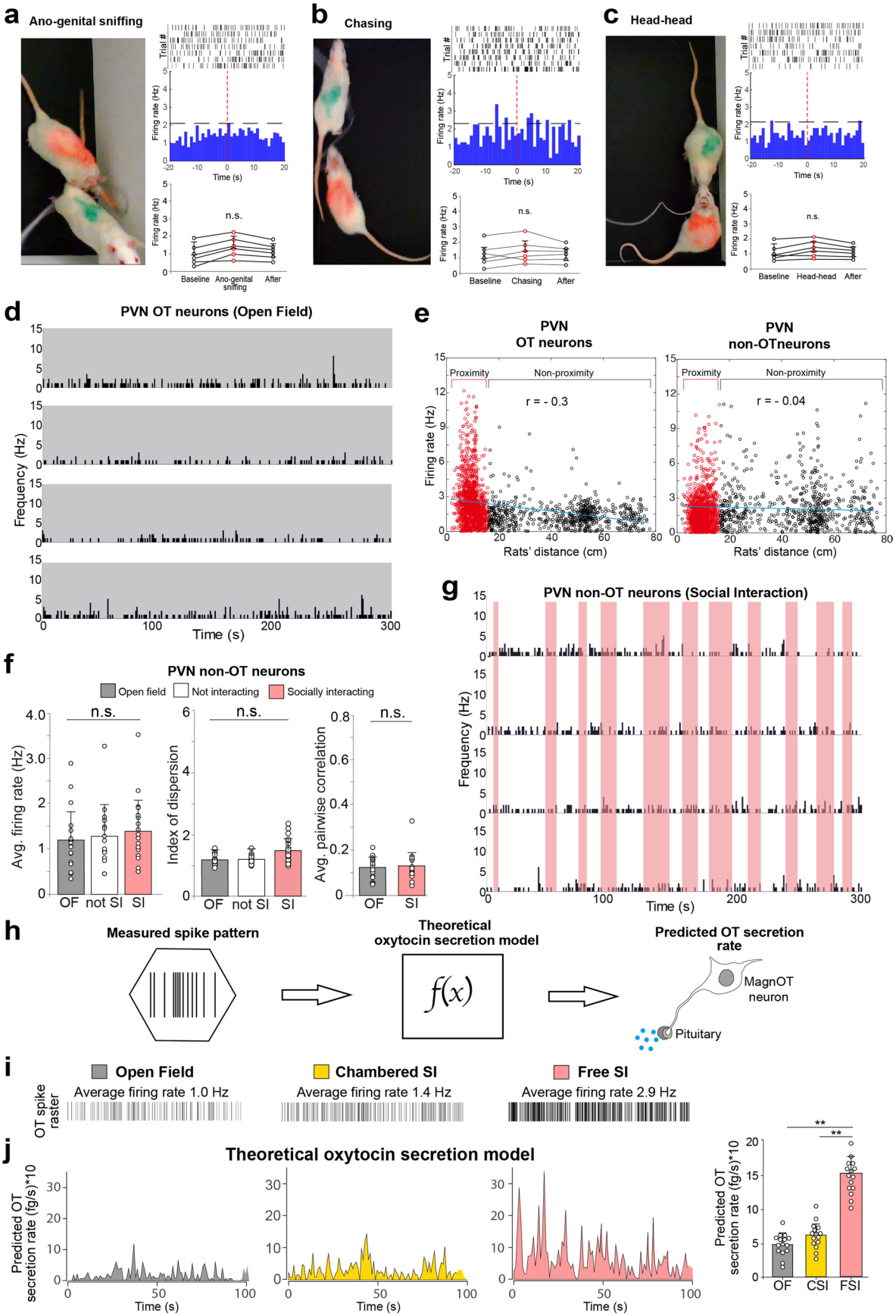

Extended Data Fig. 2 | See next page for caption.

Extended Data Fig. 2 | Analysis of social interactions, the firing rate of oxytocin and non-oxytocin PVN neurons, and activity-dependent model of oxytocin secretion. a-c, Examples of manually classified social interaction behaviors: *ano-genital sniffing*, *chasing*, *head-to-head* events. PSTHs of a single unit identified as oxytocin neurons aligned to the onset of the specific behavior. Averaged (10 s time bin) PSTHs responses before, during, and after each behavior (0 to +10 s vs. basal $P = 0.12$, $P = 0.45$, $P = 0.88$, respectively, n = 6 cells per behavior, two-sided Wilcoxon test). **d**, Example firing rate of four PVN OT neurons recorded during exploratory (OF) behavior. **e**, Linear regression of PVN OT and non-OT neuronal firing rate in relation to rat's distance in the area during FSI. OT neuronal activity shows a moderate negative correlation with distance (r = -0.3, p = 0.0092), while non-OT neurons do not show any significant correlation (r = −0.04, $P = 0.11$). **f**, Example firing rate of four PVN non-OT neurons recorded during social interaction. **g**, Average firing rate of 21 non-OT neurons from five rats (OF baseline 1.2 ± 0.2 Hz, not socially interacting (not SI) firing rate 1.2 ± 0.2 Hz, and social interacting (SI) firing rate 1.4 ± 0.2 Hz; $P = 0.83$, $P = 0.23$, $P = 0.34$, one-way ANOVA). Average index of dispersion on 1-s time bins of 21 non-OT cells (OF 1.1 ± 0.2, not SI 1.1 ± 0.2, SI 1.4 ± 0.3, $P = 0.78$, $P = 0.07$, $P = 0.11$, one-way ANOVA). Average pairwise Pearson correlation of spiking activity (1-s time bins) of 21 non-OT neurons' pairs recorded in OF and FSI ($P = 0.98$, paired two-sided t test). All data show average + SEM. **h**, Schematic illustration of the theoretical model used to estimate the amount of secreted oxytocin from axonal terminals given the measured neuronal spike pattern. **i**, Average firing rate of OT cells from rats that underwent open field (OF), CSI, and FSI tests. **j**, Predicted OT secretion rate for a representative OT cell in each condition (left). Average OT predicted secretion rate (right) in each condition (OF-CSI, $P = 0.11$, OF-FSI, ** $P = 0.005$, OF-CSI, ** $P = 0.007$, spike pattern data used for prediction are from n = 15 cells from 5 rats, one-way ANOVA followed by Tukey's post hoc test). Data represented as mean + SEM.

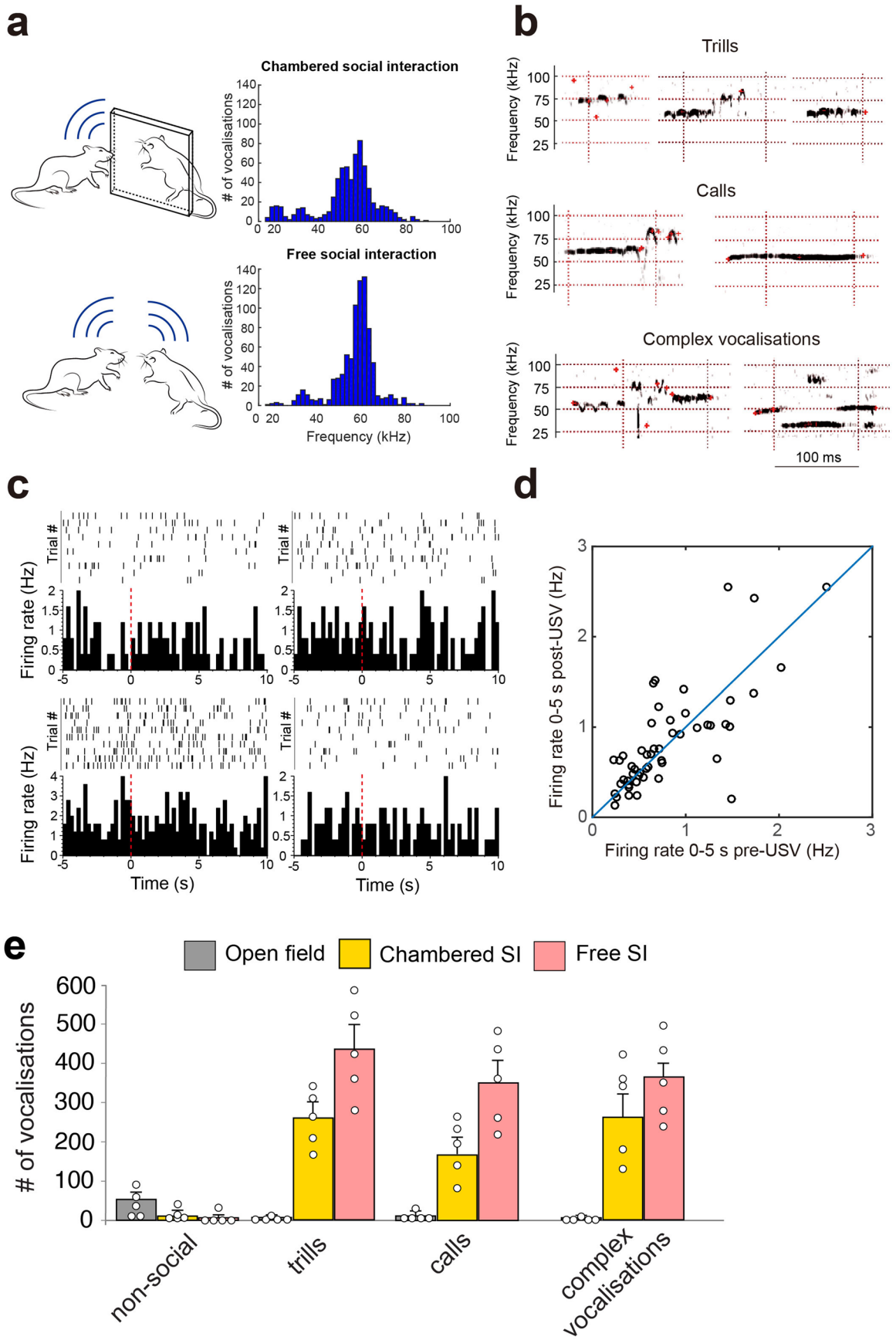

Extended Data Fig. 3 | See next page for caption.

Extended Data Fig. 3 | Ultra Sound Vocalizations (USVs) and OT neuronal activity. a, Histograms of USVs peak frequency distribution during CSI (top) and FSI (bottom). **b**, Examples of sound spectrograms showing USVs events classified as whistles, calls, or complex vocalizations. **c**, PSTHs of oxytocin neurons spiking activity aligned to USVs onset (red dashed line) show no significant time-locked correlation between them. **d**, Firing rate of oxytocin neurons 0-5 s before USV events versus 0-5 s after USV events showing no significant correlation ($P = 0.24$, n = 53 vocalisations, two-sided Wilcoxon test). **e**, Total number of USVs registered in 5 pairs (experimental and stimulus animal) of rats during OF, CSI, and FSI tests divided - according to their frequency and duration – in non-social (< 25 kHz), trills (< 10 ms), calls (> 10 ms, not modulated), and complex vocalizations (> 10 ms, frequency modulated or mixed). All data represented as mean + SEM.

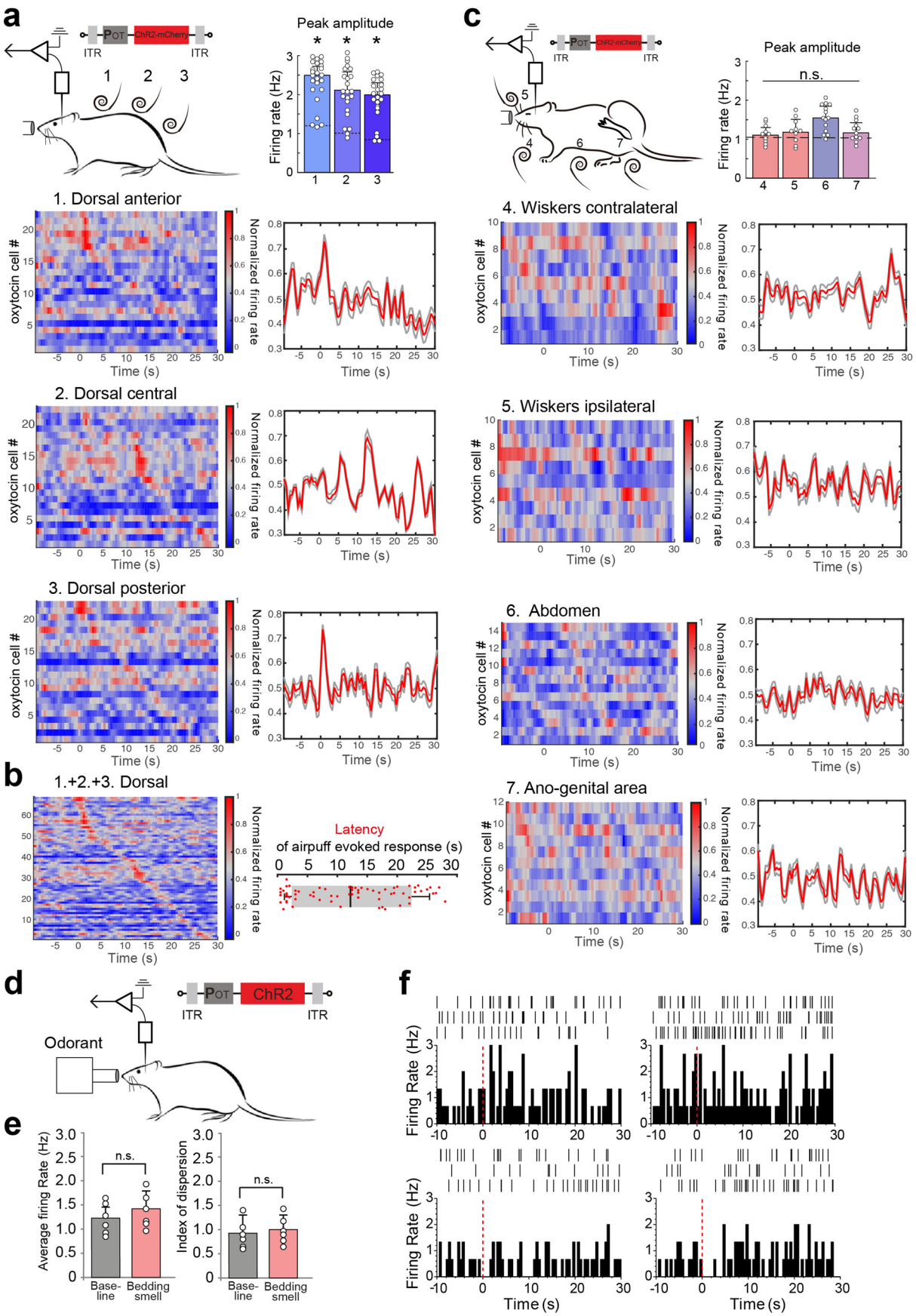

Extended Data Fig. 4 | See next page for caption.

Extended Data Fig. 4 | Oxytocin neurons response to airpuffs and to socially-related olfactory stimuli. a, Illustration of single-unit recordings of oxytocin neurons during airpuffs applied to 1. anterior, 2. central, 3. posterior (n = 23 cells from 8 rats) part of the dorsal body region. Average increase response of oxytocin neurons compared to baseline for different stimulations regions (*P = 0.017, *P = 0.025, *P = 0.021 respectively, n = 23 cells from 8 rats, one-way ANOVA followed by Bonferroni post hoc comparison). PSTHs showing single oxytocin neurons (left) and averaged (right) and response to repeated airpuffs in all stimulation sites. **b**, Combined PSTHs of 1., 2., 3., showing different response latency of oxytocin neuron to airpuff stimulations on the dorsal body area. **c**, Single-unit recordings of oxytocin neurons during airpuff stimulations on: whiskers (n = 10 cells), abdomen (n = 14 cells), and anogenital area (n = 12 cells). Average increase response of oxytocin neurons compared to baseline for different stimulation regions. PSTHs showing single oxytocin neurons (left) and averaged (right) and response to repetitive airpuff stimulations in all stimulation sites. All data represented as mean + SEM. **d**, Illustration of the experimental setup for recording oxytocin neurons activity (opto-electrodes) during presentation of olfactory stimuli. **e**, Average firing rate and index of dispersion of six oxytocin neurons 10 s before presentation of the olfactory stimuli vs 10 s after; no significant changes are detected (P = 0.34, P = 0.48, n = 6 cells from 3 rats, paired two-sided t test). Data represented as average + SEM. **f**, PSTHs of 4 (out of 6 recorded) oxytocin neurons spiking activity aligned to onset of olfactory cues (red dashed line) - urinated bedding smell; no significant changes in firing rate are detected.

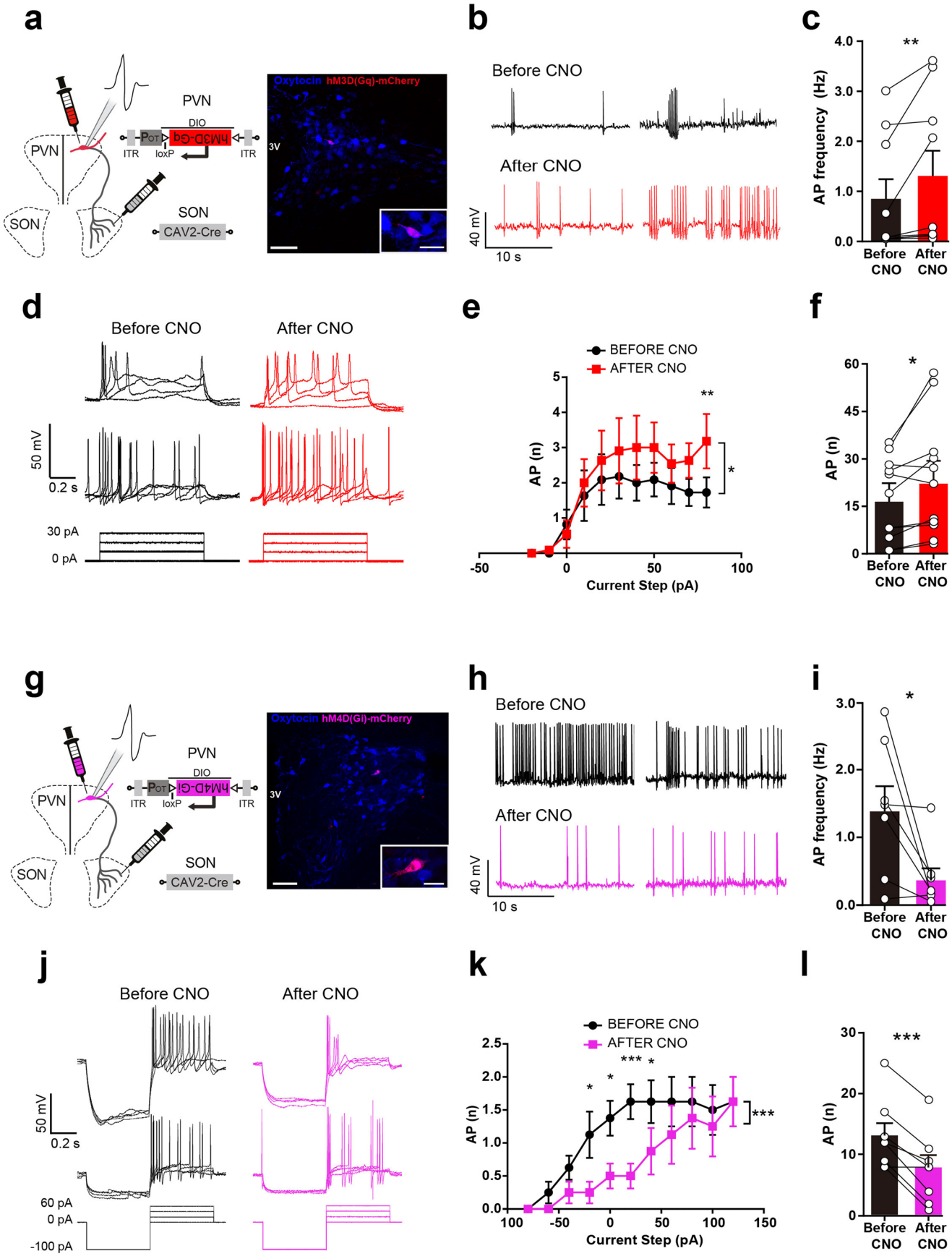

Extended Data Fig. 5 | See next page for caption.

Extended Data Fig. 5 | *Ex vivo* effects of excitatory hM3D(Gq) and inhibitory hM4D(Gi) DREADD in parvOT neurons. a, Schema of viral vectors injected for *ex vivo* recording of parvOT neurons with concomitant DREADD-Gq activation. The picture shows hM3D(Gq) (purple) and OT (blue) immunoreactivities in the PVN of one out five rats. Scale bar = 100 μm and (inset) 10 μm. **b-c**, Spontaneous response from parvOT neurons expressing hM3D(Gq) in before and after the CNO bath application; b example traces, c quantification (baseline 0.85 ± 0.39 Hz vs CNO 1.31 ± 0.51 Hz, n = 9 cells from 5 rats; $P = 0.0039$). **d-f**, Evoked responses from parvOT neurons expressing hM3D(Gq) to current injections before and after the CNO bath application; (**d**) example traces, (**e**) quantification per step (before CNO current step 80 pA 1.727 ± 0.428 nAP vs after CNO current step 80 pA 3.182 ± 0.772 nAP, n = 11; $^{**}P < 0.01$); (**f**) quantification of the average response (16.18 ± 3.89 AP vs CNO 22.55 ± 5.66 AP, n = 11 cells from 5 rats; $P = 0.0314$). **g**, Schema of viral vectors injected for *ex-vivo* recording of parvOT neurons with concomitant DREADD-Gi excitation. The picture shows hM4D(Gi) (purple) and OT (blue) immunoreactivities in the PVN of one out seven rats. Scale bar = 100 μm and (inset) 10 μm. **h-i**, Spontaneous response from parvOT neurons expressing hM4D(Gi) in before and after the CNO bath application; b example traces, c quantification (baseline 1.38 ± 0.38 Hz vs CNO 0.36 ± 0.18 Hz, n = 7 cells from 7 rats; $P = 0.0469$). **j-l**, Evoked responses from parvOT neurons expressing hM4D(Gi) to current injections before and after the CNO bath application; (**j**) example traces, (**k**) quantification per step (before CNO current step 20 pA 1.625 ± 0.263 nAP vs after CNO current step 20 pA 0.5 ± 0.189 nAP, n = 8; $^{***}P < 0.001$); **l**, quantification of the average response (baseline 13 ± 2.02 AP vs CNO 7.75 ± 2.03 AP, n = 8 cells from 7 rats; p = 0.0007). All results are expressed as average ± SEM. The statistical significances: * $P < 0.05$; ** $P < 0.01$; *** $P < 0.001$ (two-sided Wilcoxon test: c and i; Two-way ANOVA followed by a Holm-Sidak post hoc test: e and k; Paired two-sided t test: f and l). Open circles indicate individual cells.

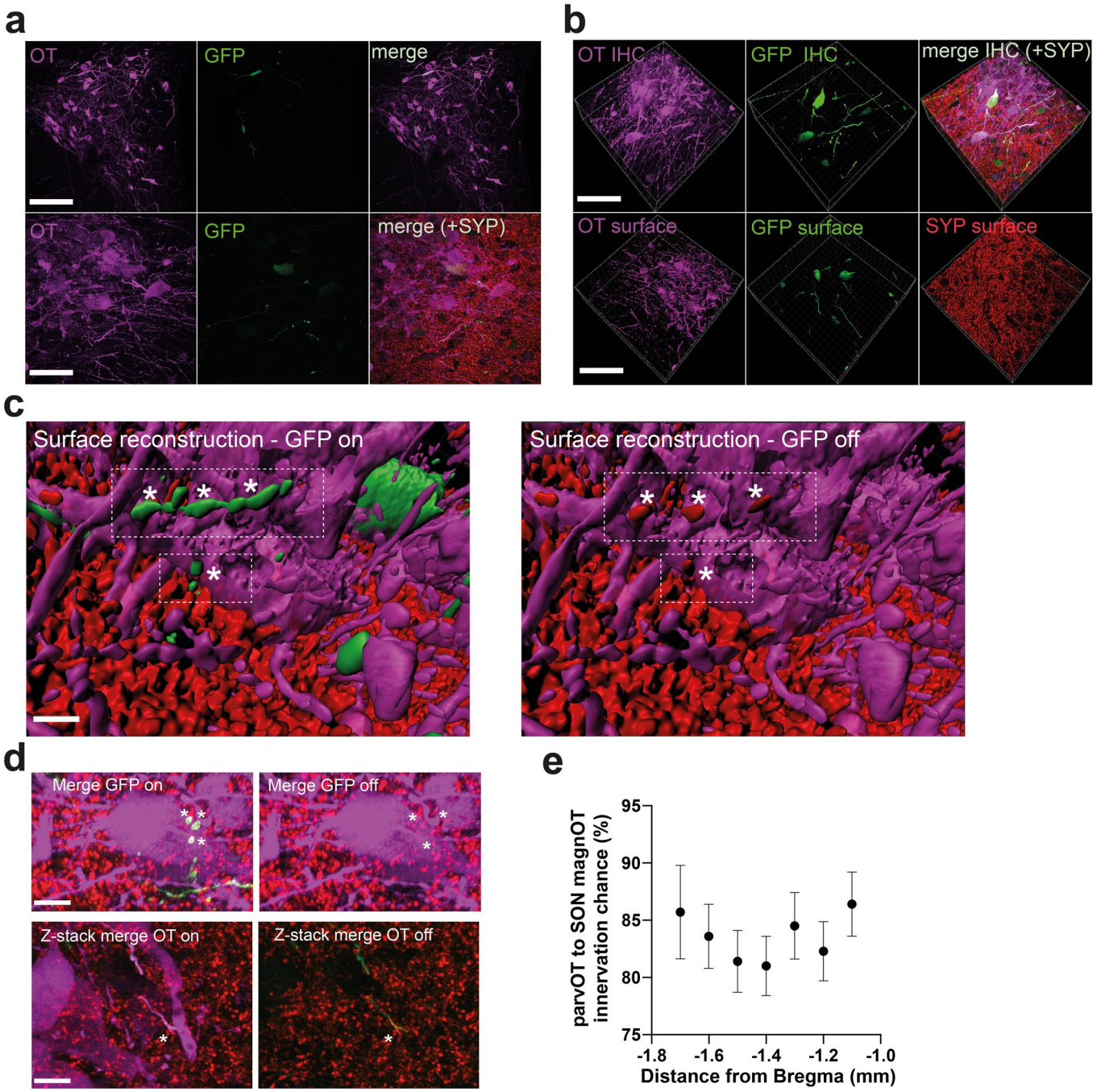

Extended Data Fig. 6 | Three-dimensional reconstruction and assessment of parvOT-magnOT connectivity. a, Confocal images show specific labeling of parvOT neurons using CAV2-Cre in combination with OTp-DIO-GFP. Top panel shows a representative PVN (one out of three independent experiments, n = 3 rats) image with 2 labeled parvOT neurons. Bottom panel shows an image with higher magnification and overlay with synaptophysin (SYN). OT = purple, GFP = green, SYN = red. Scale bars = 200 µm (top panel) and 50 µm (bottom panel). **b**, Images show raw fluorescent confocal z-stacks and surface reconstruction of individual fluorescent channels (one out of three independent experiments, n = 3 rats). The top panel shows fluorescent signals of OT, GFP and merge (+SYN). The bottom panel shows the same channels with applied surface reconstruction. Bottom images have been vertically flipped to enhance visualization of the reconstructed channels. Scale bars = 75 µm. **c**, Images show the IMARIS three-dimensional surface reconstruction of OT, GFP and SYN. Boxes with dashed lines and asterisks indicate the overlap of GFP and SYN. In the right panel the overlap between OT (purple) and GFP (green) has been manually removed to visualize the GFP/SYN (green/red) overlap (n = 169 cells from 3 rats). Scale bar = 10 µm. **d**, Confocal images show synaptic contact of parvOT neurons with magnOT somata and dendrites. Top panel shows axo-somatic contact. Bottom panel shows axo-dendritic contact using a high magnification confocal z-stack. Asterisks indicate synaptic contact. Scale bars = 10 µm. **e**, Quantification of SON OT neuron chance to receive innervation by parvOT neurons in respect to their rostro-caudal location (n = 169 cells from 3 rats). All data are presented as mean ± SEM.

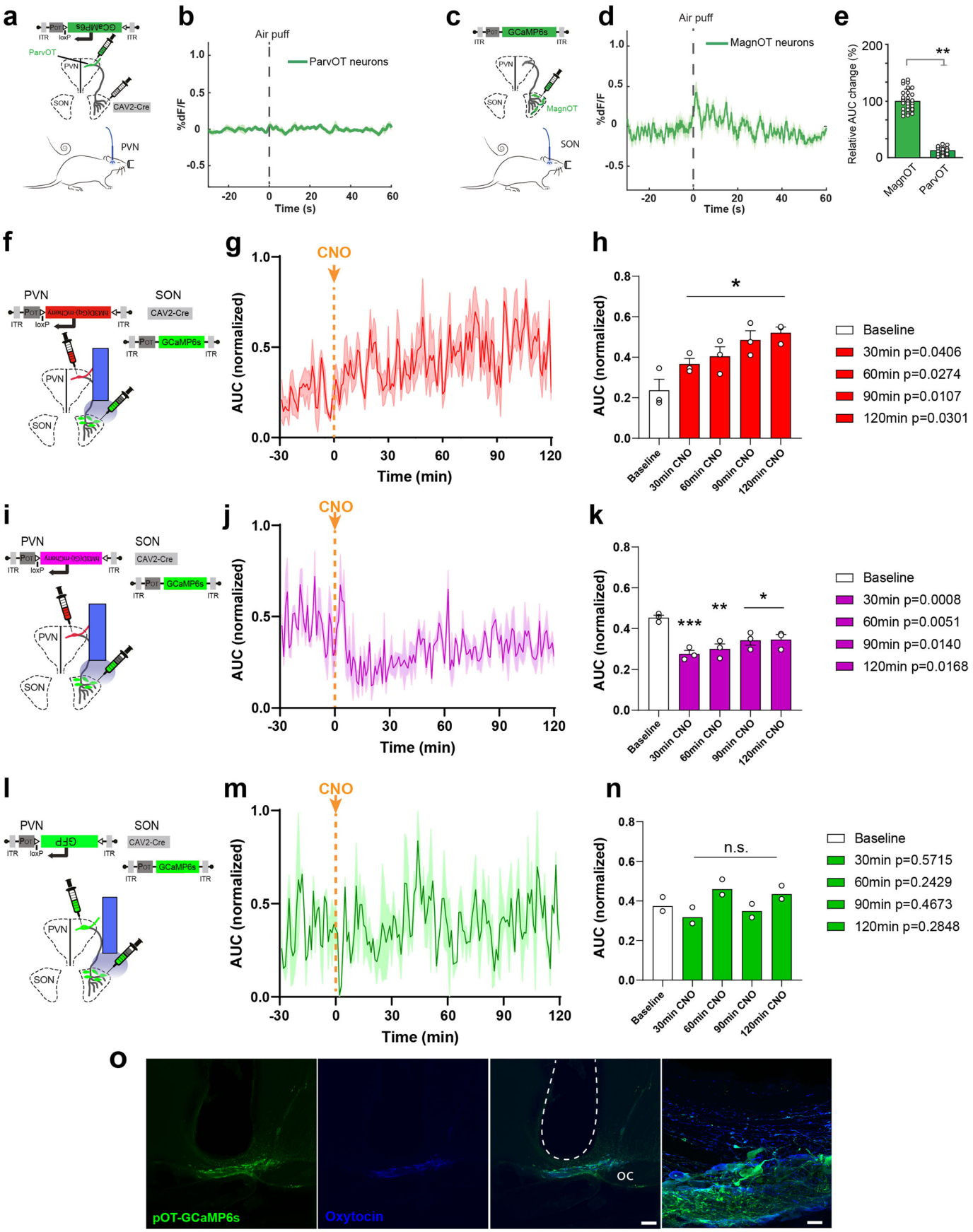

Extended Data Fig. 7 | See next page for caption.

Extended Data Fig. 7 | Fiber photometry recording of PVN parvOT neurons and SON magnOT neurons with chemogenetic manipulation of parvOT neurons. a-b, Schema of viral vectors injected (CAV2-Cre in the SON and OTp-DIO-GCaMP6s in the PVN) and implanted optic fiber for fiber photometry recording of PVN parvOT neurons (a). No Ca^{2+} transient nor changes in Ca^{2+} signal upon 'airpuff' stimulation were detected when recording parvOT neurons exclusively (b, solid line: average, shaded area: SEM, n = 3 rats). **c-d**, Schema of viral vectors injected and implanted optic fiber for fiber photometry recording of SON magnOT neurons (c). Examples of fiber photometry-based Ca^{2+} signals of SON magnOT population during airpuff stimulation (d); the graphic is an average of 33 airpuff responses (11 airpuffs per animal, n = 3 rats). **e**, Relative change in the area under the curve (AUC) 0-30 s after airpuffs with respect to 30 s before the stimuli, of SON magnOT vs. parvOT neurons (solid line: average, shaded area: SEM, n = 33 airpuffs from 3 rats, ** $P = 0.008$, unpaired two-sided t test). Data show mean + SEM. **f-g-h**, Schema of viral vectors injected and implanted optic fiber for fiber photometry recording (f) of SON OT neurons with concomitant DREADD-Gq activation of parvOT neurons. Normalized area under the curve (AUC) of GCaMP6s signal (g, solid line: average, shaded area: SEM, 1 min bin size) of SON OT neurons showing increase of cells activities after parvOT activation mediated by CNO i.p. injection (indicated by arrow). 30-min averaged AUC (h) showing a gradual increase in cellular activity and lasting at least 120 min (* $P = 0.0406$, * $P = 0.0274$, * $P = 0.0107$, * $P = 0.0301$, n = 3 rats, two-way ANOVA Tukey's corrected post-hoc comparison). Data show mean + SEM. **i-j-k**, Schema of viral vectors injected and implanted optic fiber for fiber photometry recording (i) of SON OT neurons with concomitant DREADD-Gi inhibition of parvOT neurons. Normalized area under the curve (AUC) of GCaMP6s signal (j, solid line: average, shaded area: SEM, 1 min bin size) of PVN OT neurons showing a decrease of cellular activity after parvOT inhibition mediated by i.p. CNO injection (indicated by arrow). 30-min averaged AUC (k) shows a sharp decrease in cellular activity that lasts at least 60 min and then gradually recovers (*** $P = 0.0008$, ** $P = 0.0051$, * $P = 0.0140$, * $P = 0.0168$, n = 3 rats, two-way ANOVA Tukey's corrected post-hoc comparison). Data show mean + SEM. **l-m-n**, Schema of viral vectors injected and implanted optic fiber for fiber photometry recording (l) of SON OT neurons in control animals (DREADD-free) expressing GFP in parvOT neurons. Normalized area under the curve (AUC) of GCaMP6s signal (m, solid line: average, shaded area: SEM, 1 min bin size) of PVN OT neurons showing no significant changes in Ca^{2+} signal upon CNO injection. No significant changes are detected in 30-min averaged AUC (n) up to 120 min ($P = 0.5715$, $P = 0.2429$, $P = 0.4673$, $P = 0.2848$, n = 2 rats, two-way ANOVA Tukey's corrected post-hoc comparison). Data show mean values. **o**, Panels of an immunostained section of the SON (one of out of eight independent experiments) showing post-hoc verification of implanted optic fiber above the SON and co-localization of immunoreactive, GCaMP6s (green), oxytocin (blue), and merged channels. Scale bar 100 μm and 10 μm (inset).

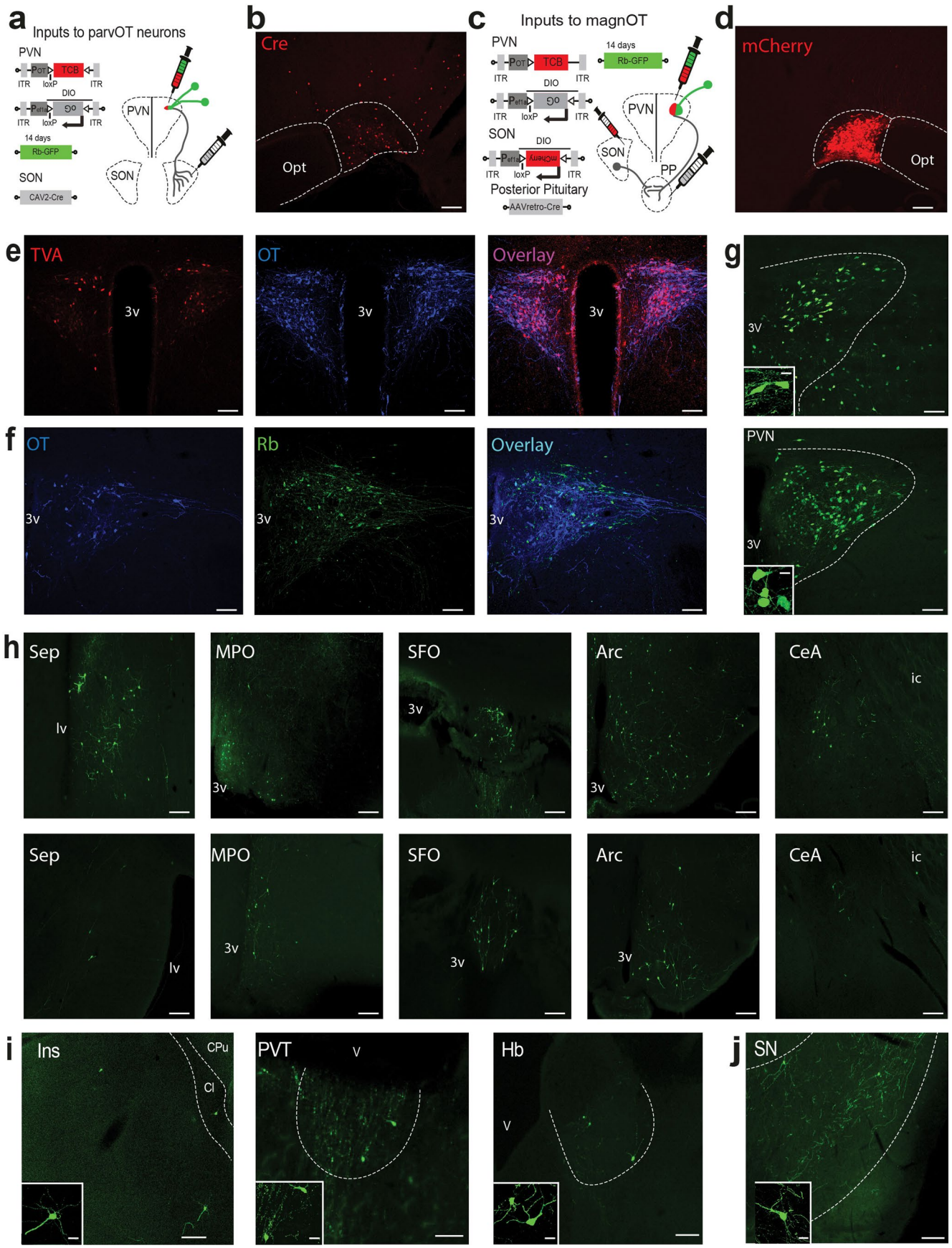

Extended Data Fig. 8 | See next page for caption.

Extended Data Fig. 8 | Inputs to parvOT and magnOT neurons. a, c, Virus injection strategy to retrotrace inputs from parvOT and magnOT neurons, respectively and to control injection sites of Cre (n = 5 rats). **b, d**, Injection site of CAV2-Cre in SON and of AAVretro-Cre in PP were confirmed by staining for Cre or mCherry in SON (n = 5 rats). **e**, Immunofluorescence for mCherry (red, fused to TVA), OT (blue) and overlay of the PVN from a rat injected with rAAV-OTp-TCB (n = 2 rats). **f**, Immunofluorescence for OT (blue), GFP (Green) and overlay of the PVN from a rat injected with rAAV-OTp-TCB, and Rb-GFP two weeks later (n = 2 rats). **g**, Injection site of rabies in parvOT (Top) and magnOT (bottom) groups (n = 5 rats). **h**, Epifluorescence microscope images showing neurons monosynaptically retrolabelled by Rabies-GFP in various brain areas projecting to both parvOT and magnOT neurons. Top line: neurons projecting to parvOT neurons; Bottom line: neurons projecting to magnOT neurons (n = 5 rats). **i, j**, Epifluorescence microscope images showing neurons monosynaptically retrolabelled by Rabies-GFP in brain areas projecting specifically to parvOT (i) or magnOT neurons (j) (n = 5 rats). All scale bars = 100 μm. All scale bars in insert = 10 μm. Brain areas legend: Amygdala: AMY, Arcuate hypothalamic nucleus: Arc, Bed nucleus of stria terminalis: NST, Cingulate cortex: CgC, Claustrum: Cl, Dorsal raphe nucleus: DRN, Dorsal tenia tecta: DTT, Dorsomedial hypothalamic area: DMH, Habenular nucleus: Hb, Horizontal limb of diagonal band nucleus: HDB, Infralimbic cortex: ILC, Insular cortex: Ins, Lateral hypothalamic area: LH, Lateral lemniscus nucleus: LMN, Lateral septal nucleus: SEP, Mammillary body: MMB, Medial preoptic area: MPO, Median raphe nucleus: MRN, Nucleus accumbens: NAC, Orbital cortex: OC, Parabrachial nucleus: PBN, Paraventricular thalamus: PVT, Pedunculopontine tegmental nucleus: PPT, Periaqueductal gray area: PAG, Posterior hypothalamic nucleus: PH, Posterior intralaminar thalamus: PIL, Prelimbic cortex: PLC, Raphe magnus nucleus: RMg, Subfornical organ:SFO, Substancia nigra: SN, Vascular organ of lamina terminalis: OVLT, Ventral Subiculum: VS, Zona incerta: ZI.

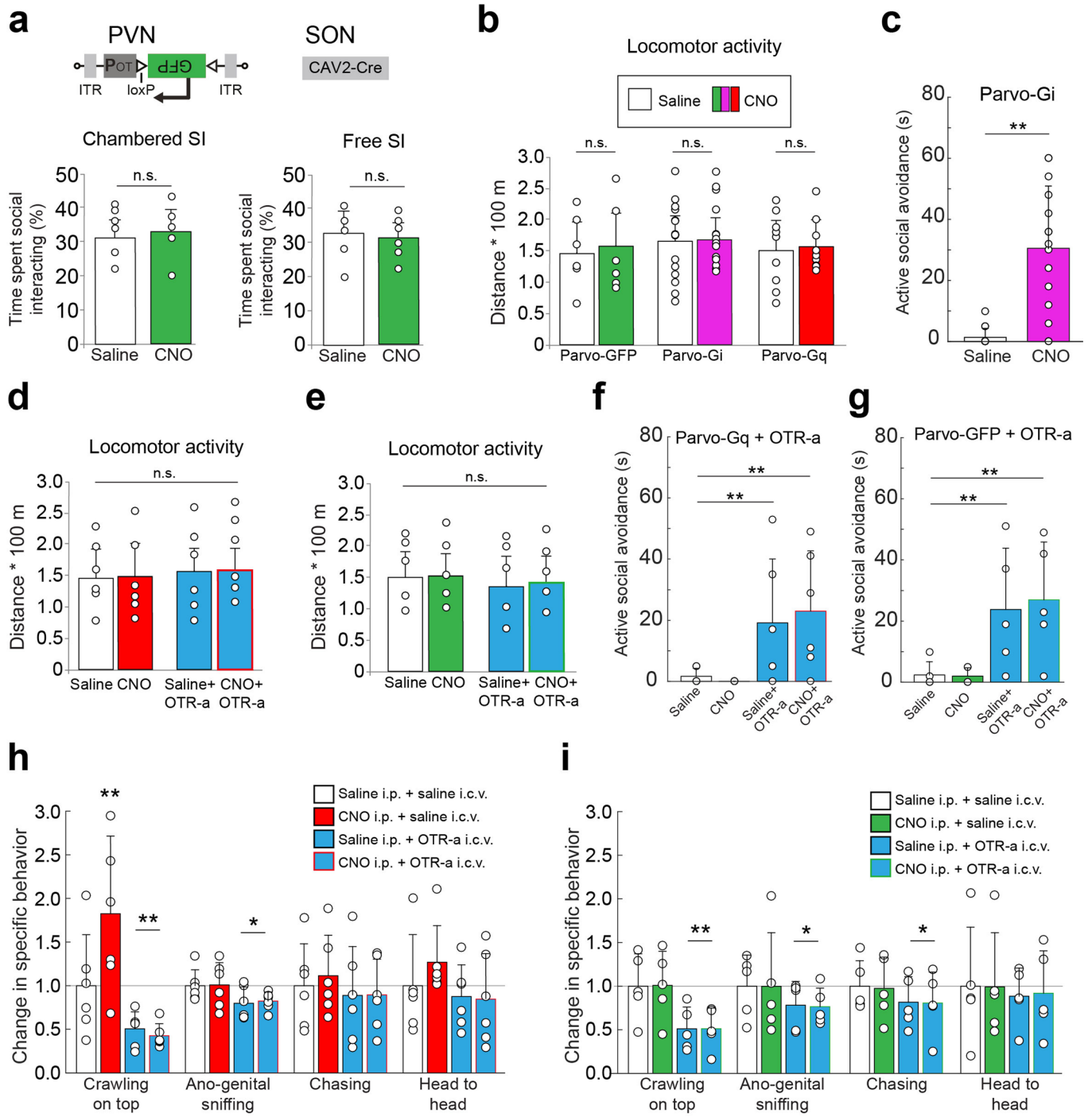

Extended Data Fig. 9 | Effects of DREADD activation of parvocellular oxytocin neurons on social behaviors. a, Parvocellular oxytocin-GFP control group: time spent by rats injected with saline or CNO socially interacting with conspecific stimulus in CSI ($P = 0.34$) and FSI session ($P = 0.29$, n = 6 rats, paired two-sided t test). **b**, CNO does not affect locomotor activity: average distance run by experimental rats (n = 6 rats GFP group, n = 15 rats Parvo-Gi group, n = 9 rats Parvo-Gq group) injected with saline or CNO during an open field (OF) test. No significant changes were detected, one-way ANOVA Tukey's corrected post-hoc comparison. **c**, Quantification of 'active social avoidance' behavior of experimental rat (actively escaping from stimulus rat, which is trying to interact) expressing inhibitory DREADD hM4D(Gi) in parvOT neurons and injected either with saline (control) or CNO. The total time of free social interaction session is 5 minutes. ** $P = 0.0096$, n = 15 rats, paired two-sided t test). **d-e**, OT receptor antagonist (OTR-a), CNO, or both do not affect locomotor activity: average distance run by experimental rats (d: $P = 0.79$, n = 6 rats saline/CNO/saline, P = 0.92 n = 6 rats saline/CNO/OTR-a; e: $P = 0.73$, n = 5 rats saline/CNO/saline, p = 0.64, n = 5 rats saline/CNO/OTR-a) injected with saline/CNO/OTR-a during an open field (OF) test. One-way ANOVA Tukey's corrected post-hoc comparison. **f-g**, Quantification of 'active social avoidance' behavior of experimental rat after administration of saline/CNO/OTR-a. Infusion of OTR-a induced an increase of avoidance behavior (Parvo-Gq: **$P = 0.0027$, **$P = 0.0018$, n = 6 rats per group, Parvo-GFP: **$P = 0.0042$, **$P = 0.0013$, n = 5 rats per group, one-way ANOVA Tukey's corrected post-hoc comparison). **h-i**, Time spent in different subtype of social behavior of experimental rat expressing excitatory DREADD hM3D(Gq) (h) or GFP (i) in parvOT neurons after administration of saline/CNO/OTR-a. Crawling on top behavior was the subtype most affected by parvOT neurons chemogenetic activation and by infusion of OTR-a (Parvo-Gq: ** $P = 0.01$, **$P = 0.004$, *$P = 0.023$, n = 6 rats per group, Parvo-GFP: **$P = 0.006$, *$P = 0.035$, *$P = 0.047$, one-way ANOVA Tukey's corrected post-hoc comparison). All data represented as mean + SEM.

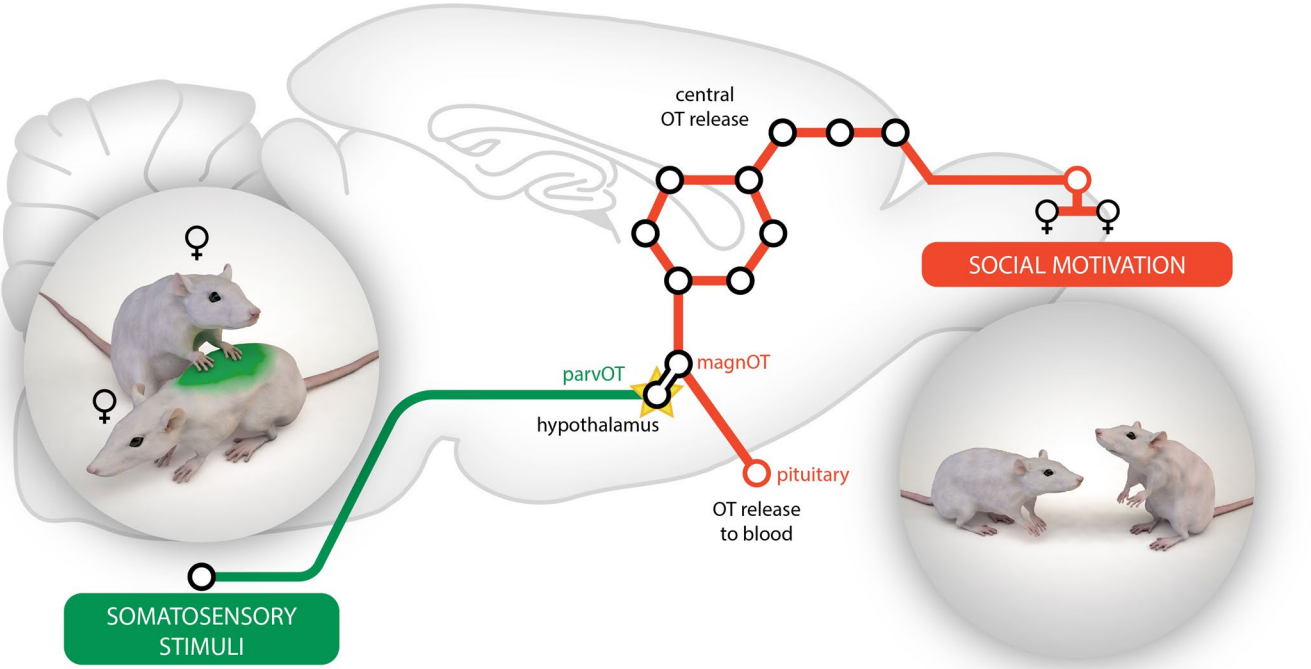

Extended Data Fig. 10 | Working hypothesis. Non-nociceptive signals ('social touch') arising from stimulation of dorsal body parts of interacting virgin female rats converge onto hypothalamic parvocellular oxytocin neurons via ascending pathways. As a consequence, the somatosensory-driven activation of parvocellular oxytocin neurons is transmitted to magnocellular oxytocin neurons inducing central oxytocin release in the social-relevant forebrain areas (as schematically depicted by circles representing nine amino acids in the oxytocin molecule), to support motivated social communication between female conspecifics.

nature research

Corresponding author(s): Valery Grinevich

Last updated by author(s): Jun 7, 2020

Reporting Summary

Nature Research wishes to improve the reproducibility of the work that we publish. This form provides structure for consistency and transparency in reporting. For further information on Nature Research policies, see Authors & Referees and the Editorial Policy Checklist.

Statistics

For all statistical analyses, confirm that the following items are present in the figure legend, table legend, main text, or Methods section.

n/a	Confirmed	
☐	☒	The exact sample size (*n*) for each experimental group/condition, given as a discrete number and unit of measurement
☐	☒	A statement on whether measurements were taken from distinct samples or whether the same sample was measured repeatedly
☐	☒	The statistical test(s) used AND whether they are one- or two-sided *Only common tests should be described solely by name; describe more complex techniques in the Methods section.*
☐	☒	A description of all covariates tested
☐	☒	A description of any assumptions or corrections, such as tests of normality and adjustment for multiple comparisons
☐	☒	A full description of the statistical parameters including central tendency (e.g. means) or other basic estimates (e.g. regression coefficient) AND variation (e.g. standard deviation) or associated estimates of uncertainty (e.g. confidence intervals)
☐	☒	For null hypothesis testing, the test statistic (e.g. *F*, *t*, *r*) with confidence intervals, effect sizes, degrees of freedom and *P* value noted *Give P values as exact values whenever suitable.*
☒	☐	For Bayesian analysis, information on the choice of priors and Markov chain Monte Carlo settings
☒	☐	For hierarchical and complex designs, identification of the appropriate level for tests and full reporting of outcomes
☐	☒	Estimates of effect sizes (e.g. Cohen's *d*, Pearson's *r*), indicating how they were calculated

Our web collection on statistics for biologists contains articles on many of the points above.

Software and code

Policy information about availability of computer code

Data collection	Ex-vivo electhrophysiological data were collected using pClamp 10 (Axon Instrument). In-vivo electrophysiological data were collected using Open-Ephys GUI (v0.4), software that is public available (http://www.open-ephys.org/gui). Behavioral experiments were recorded using Ethovision XT 11.5 (Noldus).
Data analysis	Data analysis was performed using Clampfit 10.7 (Molecular Devices, USA), Mini analysis 6 (Synaptosoft, USA), Avisoft-SASlab Pro 5.0 (Avisoft Bioacustic, Germany), Offline Sorter (Plexon, USA), and Neuroexplorer 3 (Nex Technologies, USA). Statistical analysis was performed using SigmaPlot 11 (Systat, USA), GraphPad Prism 7.05 (GraphPad Software, San Diego, California, USA), and custom scripts written in MATLAB R2015a (MathWorks, USA). All codes and algorithms used in the analysis are available from the corresponding author upon reasonable request.

For manuscripts utilizing custom algorithms or software that are central to the research but not yet described in published literature, software must be made available to editors/reviewers. We strongly encourage code deposition in a community repository (e.g. GitHub). See the Nature Research guidelines for submitting code & software for further information.

Data

Policy information about availability of data

All manuscripts must include a data availability statement. This statement should provide the following information, where applicable:

- Accession codes, unique identifiers, or web links for publicly available datasets
- A list of figures that have associated raw data
- A description of any restrictions on data availability

The data that support the findings of this study are available from the corresponding author upon reasonable request.

Field-specific reporting

Please select the one below that is the best fit for your research. If you are not sure, read the appropriate sections before making your selection.

☒ Life sciences ☐ Behavioural & social sciences ☐ Ecological, evolutionary & environmental sciences

For a reference copy of the document with all sections, see nature.com/documents/nr-reporting-summary-flat.pdf

Life sciences study design

All studies must disclose on these points even when the disclosure is negative.

Sample size	Sample size was determined to be adequate based on the magnitude and consistency of measurable differences between groups and/or experimental conditions.
Data exclusions	Data obtained from 15 rats were excluded from the analysis due to mistargeting or insufficient expression of viral vectors.
Replication	Experiments were repeated so that our data are based on at least three independent experiments with similar results. All attempts at replication were successful. The precise number of repeats are given in the text or in figure legends.
Randomization	Randomization was used to assign brain samples and animals to experimental groups whenever possible, with the constraint that in social behavior experiments rats had to be between unknown conspecifics, as described in Method section on page 44.
Blinding	Most of the measurements are made using a machine, and are not subject to operator bias, with the exception of manual scoring of social behaviors from videos; in this case, all scoring were done by a researcher (different from the one who performed the experiment) that was blind to treatment conditions.

Reporting for specific materials, systems and methods

We require information from authors about some types of materials, experimental systems and methods used in many studies. Here, indicate whether each material, system or method listed is relevant to your study. If you are not sure if a list item applies to your research, read the appropriate section before selecting a response.

Materials & experimental systems

n/a	Involved in the study
☐	☒ Antibodies
☐	☒ Eukaryotic cell lines
☒	☐ Palaeontology
☐	☒ Animals and other organisms
☒	☐ Human research participants
☒	☐ Clinical data

Methods

n/a	Involved in the study
☒	☐ ChIP-seq
☒	☐ Flow cytometry
☒	☐ MRI-based neuroimaging

Antibodies

Antibodies used	Primary antibodies: anti-oxytocin (PS38, mouse, kindly provided by Dr. Harold Gainer, NIH, Bethesda, USA), anti-oxytocin (T-5021, guinea pig, 1:50,000; Peninsula) anti-synaptophysin (ab32127, rabbit, 1:1,000, Abcam), anti-Ds-Red (#632397, rabbit, 1:1000, Clontech), anti-GFP (ab13970, chicken, 1:1000, Abcam), anti c-Fos (#9F6, rabbit, 1:500, Cell Signaling), anti-Fluorogold (NM-101, guinea pig, 1:1000, Protos Biotech), anti-Cre (#69050, mouse, 1:2000, Novagen). Secondary antibodies: CY3-conjugated (711-165-152, 1:500, Jackson Immuno-Reseach), CY5-conjugated (115-175-146, 1:500, Jackson Immuno-Research), Alexa 488 (A11039, 1:500, Invitrogen), Alexa 594 (A11012, 1:500, Invitrogen), Alexa 594 (715-585-151, 1:500, Jackson Immuno-Research), Alexa 647 (713-645-147, 1:500, Jackson Immuno-Research).
Validation	Validation of anti-oxytocin (PS38) immunohistochemistry in rat was first reported in (Ben-Barak et al., J. of Neurosci., 1985). Validation of anti-oxytocin (T-5021), anti-Ds-Red (#632397), anti-GFP (ab13970), anti c-Fos (#9F6), anti-Fluorogold (NM-101), immunohistochemistry in rat was reported in (Hasan et al., Neuron, 2019). Validation of anti-synaptophysin (ab32127) immunohistochemistry in rat was reported in (Lecanu et al., Neuroscience, 2010). Validation of anti-Cre (#69050) immunohistochemistry in mouse was reported in (Rajji et al., J. of Neurosci., 2006).

Eukaryotic cell lines

Policy information about cell lines

Cell line source(s)	Human embryonic kidney (HEK) 293T cell line was originally purchased from Addgene, USA (catalog number #240073).

Authentication	Cells authentication was done by microscopic inspection.
Mycoplasma contamination	All cell lines were tested negative for mycoplasma contamination.
Commonly misidentified lines (See ICLAC register)	No commonly misindentified cell lines were used in this study.

Animals and other organisms

Policy information about studies involving animals; ARRIVE guidelines recommended for reporting animal research

Laboratory animals	Four to eight-week old female Wistar rats purchased from Janvier, France and were housed under standard laboratory conditions: 12-h light/dark cycle, lights on at 07:00, 22-24 °C, 50 +/- 5% humidity, free access to food and water.
Wild animals	The study did not involve wild animals.
Field-collected samples	The study did not involve samples collected from the field.
Ethics oversight	All experiments were conducted under animal lisence G-102/17 authorized by the German Animal Ethics Committee of the Baden Württemberg (Regierungspräsidium Karlsruhe, Germany) and in accordance with the German low, under license 3668-2016011815445431 from the French Ministry, and under EU regulations.

Note that full information on the approval of the study protocol must also be provided in the manuscript.